

1

2

3

4

5 **Mitochondrial proline catabolism activates Ras1/cAMP/PKA-induced**  
6 **filamentation in *Candida albicans***

7

8

9 **Fitz Gerald S. Silao, Meliza Ward, Kicki Ryman, Axel Wallström, Björn Brindefalk, Klas**  
10 **Udekwu and Per O. Ljungdahl\***

11

12

13 Department of Molecular Biosciences, The Wenner-Gren Institute, Stockholm University,  
14 Stockholm, Sweden

15

16 Running title: Mitochondrial-dependent morphogenesis

17

18

19

20 \*Corresponding author

21 E-mail: per.ljungdahl@su.se

22 **Abstract**

23 Amino acids are among the earliest identified inducers of yeast-to-hyphal transitions in *Candida*  
24 *albicans*, an opportunistic fungal pathogen of humans. Here, we show that the morphogenic  
25 amino acids arginine, ornithine and proline are internalized and metabolized in mitochondria via  
26 a *PUT1*- and *PUT2*-dependent pathway that results in enhanced ATP production. Elevated ATP  
27 levels correlate with Ras1/cAMP/PKA pathway activation and Efg1-induced gene expression.  
28 The magnitude of amino acid-induced filamentation is linked to glucose availability; high levels  
29 of glucose repress mitochondrial function thereby dampening filamentation. Furthermore,  
30 arginine-induced morphogenesis occurs more rapidly and independently of Dur1,2-catalyzed  
31 urea degradation, indicating that mitochondrial-generated ATP, not CO<sub>2</sub>, is the primary  
32 morphogenic signal derived from arginine metabolism. The important role of the SPS-sensor of  
33 extracellular amino acids in morphogenesis is the consequence of induced amino acid permease  
34 gene expression, i.e., SPS-sensor activation enhances the capacity of cells to take up  
35 morphogenic amino acids, a requisite for their catabolism. *C. albicans* cells engulfed by murine  
36 macrophages filament, resulting in macrophage lysis. Phagocytosed *put1*<sup>-/-</sup> and *put2*<sup>-/-</sup> cells do  
37 not filament and do not lyse macrophages, consistent with a critical role of mitochondrial proline  
38 metabolism in virulence.

39

## 40 **Introduction**

41 *Candida albicans* is an opportunistic fungal pathogen that commonly exists as a benign member  
42 of the human microbiome. Immunosuppression, or microbial dysbiosis, can predispose an  
43 individual to infection, enabling this fungus to initiate and develop a spectrum of pathologies,  
44 including superficial mucocutaneous or even life-threatening invasive infections [1, 2]. As a  
45 human commensal, *C. albicans* can asymptotically colonize virtually all anatomical sites in  
46 the host, each with a characteristic and unique microenvironment, with differing nutrient and  
47 microbiome compositions, physical properties, and levels of innate immune defenses [3]. The  
48 ability to colonize and infect discrete microenvironments is attributed to an array of virulence  
49 characteristics, a major one being its morphological plasticity. As a pleomorphic organism, *C.*  
50 *albicans* can assume at least three distinct morphologies: yeast-like, pseudohyphae, and true  
51 hyphae, where the latter two are commonly referred to as filamentous morphologies (for review  
52 see [4-7]). Strains that are genetically locked in either yeast or filamentous forms fail to mount  
53 infections *in vitro* and *in vivo* infection models, supporting the concept that morphological  
54 switching, rather than the specific morphology *per se*, is a requisite to virulence [4, 6, 8-10]. The  
55 environmental signals known to trigger morphogenesis in *C. albicans* reflect the conditions  
56 within the human host, such as temperature (37 °C) and CO<sub>2</sub>, alkaline pH, the presence of serum,  
57 N-acetylglucosamine, and a discrete set of amino acids.

58 Early studies examining amino acid-induced morphogenesis implicated metabolism as being  
59 important for filamentation, and the inducing effects were shown to correlate to their specific  
60 point-of-entry in metabolism [11-13]. The most potent inducers of filamentation are amino acids  
61 that are catabolized to glutamate, such as arginine and proline, which enters the TCA cycle via  
62  $\alpha$ -ketoglutarate. Importantly, arginine and proline can supply nitrogen and carbon for  
63 intermediary metabolism and their catabolism provides energy to support diverse cellular  
64 functions. Studies examining proline uptake and distribution during filamentous growth  
65 suggested that proline catabolism results in an increase in the cellular reducing potential, i.e.,  
66 enhanced levels of reduced flavoproteins were noted [11]. Several of the conclusions from these  
67 earlier studies, in particular that filamentous growth of *C. albicans* is linked to repression of  
68 mitochondrial activity [11-13], appear to conflict with more recent reports showing that

69 filamentation is accompanied by increased mitochondrial respiratory activity [14-16]. Clearly,  
70 the underlying mechanisms through which amino acids induce filamentation remain to be  
71 defined. In particular, the basis of arginine- and proline-induced morphogenesis needs to be  
72 placed in context to the current mechanistic understanding of the signaling cascades implicated  
73 in morphogenesis.

74 Among the central metabolic signaling pathways in *C. albicans* linked to morphogenesis, the  
75 best characterized are the mitogen-activated protein kinase (MAPK) and the 3'-5'-cyclic  
76 adenosine monophosphate/Protein Kinase A (cAMP/PKA) signaling systems, which activate the  
77 transcription factors Cph1 and Efg1, respectively [8, 17, 18], reviewed in [4, 7, 19, 20]. Ras1 is  
78 a small GTPase required for proper MAPK and cAMP/PKA signaling, and specifically for the  
79 induction of filamentation by amino acids and serum [21, 22], reviewed in [20, 23]. Recently,  
80 Grahl et al. have proposed that intracellular ATP levels and increased mitochondrial activity,  
81 control the activation of Ras1/cAMP/PKA pathway [14]. In this intriguing model, the adenyl  
82 cyclase (Cyr1/Cdc35) works cooperatively in a positive feedback loop with ATP as key input.  
83 Accordingly, ATP promotes Cyr1 binding to the active GTP-bound form of Ras1 thereby  
84 reducing the ability of Ira2 to stimulate the intrinsic GTPase activity of Ras1. As a consequence,  
85 enhanced Cyr1 activity leads to elevated levels of cAMP and amplification of PKA-dependent  
86 signaling, activating the effector transcription factor Efg1 and the expression of genes required  
87 for filamentous growth [24-26], reviewed in [20, 23, 27, 28].

88 Some morphogenic signals appear to bypass the requirement for Ras1 (reviewed in [27, 28]).  
89 By example, CO<sub>2</sub> is a well-characterized stimulus for morphological switching in *C. albicans*;  
90 CO<sub>2</sub> binds directly and activates Cyr1 [29]. Ghosh et al. have proposed that arginine-induced  
91 morphogenesis is the consequence of arginase (*CARI*) dependent metabolism to ornithine and  
92 urea, and subsequent urea amidolyase (*DURI,2*) dependent generation of CO<sub>2</sub> from urea [30].  
93 Also, the G protein-coupled receptor Gpr1, which has been implicated in amino acid-induced  
94 morphogenesis, does not appear to require Ras1. Gpr1-initiated signals activate Cyr1 by  
95 stimulating GTP-GDP exchange on the G $\alpha$  protein Gpa2; the active GTP-bound form of Gpa2  
96 is thought to bind to the G $\alpha$ -binding domain within the N-terminal of Cyr1 leading to enhanced  
97 cAMP production (reviewed in [20, 28]). It has been reported that Gpr1 senses the presence of

98 extracellular methionine [31] and glucose [32], however recently, lactate has been proposed to  
99 be the primary activating ligand [33]. The role of Gpr1 in amino acid-induced morphogenesis  
100 remains an open question.

101 *C. albicans* cells respond to the presence of extracellular amino acids using the plasma  
102 membrane-localized SPS (Ssy1-Ptr3-Ssy5) sensor complex [34-36]. In response to amino acids,  
103 the primary sensor Ssy1 (Csy1) is stabilized in a signaling conformation leading to Ssy5-  
104 mediated proteolytic processing of two latently expressed transcription factors, Stp1 and Stp2  
105 [34]. The processed factors efficiently target to the nucleus activating the expression of distinct  
106 sets of genes required for assimilation of external nitrogen. Stp1 regulates the expression of  
107 *SAP2*, encoding the major secreted aspartyl proteinase, and oligopeptide transporters (*OPT1* and  
108 *OPT3*); whereas Stp2, derepresses the expression of a subset of amino acid permeases (AAP)  
109 that facilitate amino acid uptake. *STP1* expression is controlled by nitrogen catabolite repression  
110 (NCR), a supra-regulatory system that represses that utilization of non-preferred nitrogen sources  
111 when preferred ones are available [37]. The endoplasmic reticulum (ER)-localized chaperone  
112 Csh3, is required for the functional expression of both Ssy1 and AAPs, and thus acts as the most  
113 upstream and downstream component of the SPS sensing pathway [35]. Strains lacking either  
114 Ssy1 or Csh3 fail to efficiently respond to the presence of extracellular amino acids and serum  
115 and exhibit impaired morphological switching [35, 36]. It has not previously been determined if  
116 the SPS-sensor induces morphogenesis directly in response to extracellular amino acids, or  
117 indirectly, the consequence of enhanced amino acid uptake and subsequent intracellular  
118 signaling events.

119 In this report, we show how amino acid-induced and SPS-sensor-dependent signals are  
120 integrated into the central signaling pathways that control yeast-to-hyphal morphological  
121 transitions in *C. albicans*. Our results indicate that the augmented levels of intracellular ATP,  
122 resulting from catabolism of proline in the mitochondria, correlate with activated  
123 Ras1/cAMP/PKA and Efg1-dependent gene expression. The magnitude of the response is  
124 sensitive to the levels of glucose in a manner consistent with glucose repression of mitochondrial  
125 function. The SPS-sensor plays an indirect, but important, role in enhancing the uptake of the  
126 inducing amino acids. Finally, we show that *C. albicans* cells express proline catabolic enzymes

127 when phagocytosed by murine macrophages, and that inactivation of proline catabolism  
128 diminishes the capacity of *C. albicans* cells to induce hyphal growth and escape engulfing  
129 macrophages.

130

## 131 **Results**

### 132 **Amino acid-induced morphogenesis is dependent on uptake**

133 We assessed the capacity of ornithine, citrulline, and the 20 amino acids commonly found in  
134 proteins to induce filamentous growth in *C. albicans*. Wildtype (WT) cells were grown as  
135 macrocolonies on MES-buffered (pH of 6.0) synthetic dextrose (2% glucose) medium containing  
136 10 mM of each individual amino acid as sole nitrogen source. As shown in **Fig. 1A**, proline and  
137 arginine strongly induced filamentous growth as evidenced by the formation of wrinkled  
138 macrocolonies. Microscopic evaluation of cells from wrinkled colonies confirmed the presence  
139 of extensive filamentous growth (mainly hyphae). Ornithine, a non-proteinogenic amino acid  
140 and a catabolic intermediate in the degradation of arginine, induced pronounced filamentous  
141 growth. Of the amino acids tested, aspartate consistently produced smooth macrocolonies  
142 comprised of round cells, exclusively yeast-like in appearance. Consequently, aspartate was  
143 chosen as a reference for subsequent studies.

144 Using quantitative RT-PCR (qRT-PCR) we analyzed the expression of known hyphae-  
145 specific genes (HSG) *ECE1*, *EED1*, *HWPI*, *UME6*, *ALS3*, *HGC1*, *SAP4*, and *SAP5* [4] in cells  
146 from colonies grown on media with arginine, proline, ornithine and aspartate. With the exception  
147 of *EED1*, the expression of HSG were clearly induced in cells grown on media with morphogenic  
148 amino acids,  $\geq 7$ -fold higher than in cells grown on aspartate (**Fig. S1**). *SAP4*, a known Efg1-  
149 regulated gene [38], exhibited the highest level of induction,  $\geq 80$ -fold higher levels than in  
150 aspartate grown cells. These experiments were repeated using liquid cultures, and the same  
151 trends were observed (data not shown). These results confirm the appropriateness of using  
152 macrocolonies to score amino acid-induced morphogenesis.

153 Next, we evaluated whether SPS-sensor activation was required for amino acid-induced  
154 morphogenesis. This was accomplished by assessing SPS-sensor dependent Stp2 processing

155 [34]. A strain carrying a functional C-terminal HA tagged Stp2 (Stp2-HA; PMRCA44) was  
156 grown in minimal ammonium-based synthetic dextrose (SD) medium, extracts were prepared 5  
157 min after induction by the indicated amino acid. Arginine (R), asparagine (N), aspartate (D),  
158 glutamine (Q), histidine (H), lysine (K), serine (S) and ornithine (Orn) efficiently activated the  
159 SPS-sensor; extracts contained the shorter processed form of Stp2 (**Fig. 1B**, upper panel). Next,  
160 we assessed Stp2-dependent promoter activation using an integrated  $P_{CAN1}$ -NanoLuc<sup>TM</sup>-PEST  
161 reporter construct; the expression of the luciferase signal is controlled by the *CAN1* promoter,  
162 which is strictly dependent on the SPS-sensor and Stp2 (**Fig. S2A and S2B**). The inclusion of  
163 the 41-amino acid PEST sequence confers a shorter NanoLuc<sup>TM</sup> lifetime, which facilitates a  
164 tighter coupling of transcription and translation [39]. Enhanced luminescence was observed only  
165 in cells induced with the amino acids giving rise to Stp2 processing (**Fig. 1B**, lower panel).  
166 Notably, proline, which induces robust filamentation, did not activate the SPS-sensor as no Stp2  
167 processing or luminescence was detected. Conversely, aspartate, which does not induce  
168 filamentous growth, robustly activated the SPS-sensor as determined by Stp2 processing and  
169 enhanced luciferase activity. These results indicate that amino acid-induced morphogenesis is  
170 not obligatorily coupled to SPS-sensor signaling.

171 The contribution of signals derived from the SPS sensing pathway on filamentation induced  
172 by arginine, ornithine and proline was examined. Arginine, a potent inducer of the SPS-sensor  
173 (**Fig. 1B**), induced filamentation in an SPS-sensor independent manner; filamentation was  
174 observed in mutants lacking components of the SPS sensing pathway (**Fig. 1C**). By contrast,  
175 ornithine, also a potent inducer of the SPS-sensor, induced filamentous growth in a strictly SPS-  
176 sensor- and Stp2-dependent manner (**Fig. 1C**). Notably, Stp1, a transcription factor that induces  
177 genes required for extracellular protein utilization, is not required for ornithine-induced  
178 filamentation. Proline, which does not induce SPS-sensor signaling, promoted filamentous  
179 growth in an SPS-sensor independent manner (**Fig. 1C**). Importantly, the filamentation was  
180 greatly reduced in cells lacking *CSH3* (*csh3Δ/Δ*), a gene encoding a membrane-localized  
181 chaperone required for the functional expression of Ssy1 and most amino acid permeases [35,  
182 36] (**Fig. 1C**), clearly suggesting that amino acid uptake is required for amino acid-induced  
183 morphogenesis.

184 The clear requirement of the SPS-sensor in facilitating ornithine-induced filamentation  
185 provided the opportunity to rigorously test the notion that uptake is essential. Based on the  
186 knowledge that amino acid permease-dependent uptake is dependent on Stp2 and not Stp1, we  
187 used the CRISPR/Cas9 system to introduce *ssy1* null mutations in strains expressing  
188 constitutively active Stp2 (*STP2\**) or Stp1 (*STP1\**) (**Fig. S3A**). The results clearly show that  
189 *STP2\**, but not *STP1\** (**Fig. 1D**), bypasses the *ssy1* null mutation, indicating that the permease  
190 responsible for ornithine uptake is indeed encoded by a SPS-sensor and Stp2 controlled gene.  
191 Similarly, SPS-sensor dependence was observed for the inducing amino acids alanine,  
192 glutamine, and serine (data not shown). Together, these results indicate that amino acid-induced  
193 filamentous growth is dependent on the uptake of the inducing amino acid.

194  
195 **Amino acid-induced morphogenesis is dependent on catabolism and Ras1/cAMP/PKA**  
196 **signaling**

197 Two core signaling pathways, i.e., MAPK and cAMP/PKA, are known to transduce metabolic  
198 signals that affect filamentous growth (**Fig. 2A**). We evaluated the capacity of amino acids to  
199 induce filamentation in cells carrying null alleles of *RAS1* and the effector transcription factors,  
200 *CPH1* and *EFG1* diagnostic for MAPK and cAMP/PKA signaling, respectively [8, 18, 40](**Fig.**  
201 **2B**). Similar to wildtype, *cph1* $\Delta/\Delta$  cells were wrinkled in appearance, indicating that amino acid  
202 induced filamentation was independent of MAPK signaling. By contrast, the colonies derived  
203 from *ras1* $\Delta/\Delta$  and *efg1* $\Delta/\Delta$  cells were smooth. As expected, the *efg1* $\Delta/\Delta$  *cph1* $\Delta/\Delta$  double mutant  
204 strain also formed smooth colonies. These results indicate that the inducing signals are  
205 transduced by the cAMP/PKA pathway. A clear dependence on Ras1/cAMP/PKA signaling was  
206 also observed for other inducing amino acids, i.e., alanine, glutamine, and serine (data not  
207 shown). Our results demonstrating that amino acid-induced morphogenesis is strictly dependent  
208 on Ras1 is contrary to current models that postulate that amino acids-initiated signals are  
209 transduced by Gpr1/Gpa2 (reviewed in [20, 28]. According to these models, amino acid signaling  
210 should be Ras1 independent.

211 Our results regarding the clear Ras1-dependence suggested that amino acid-initiated signals

212 promote GTP-GDP exchange. To test this notion, we assessed the levels of Ras1-GTP in cells  
213 after induction by amino acids (**Fig. 2C**). Our results clearly show that in contrast to cells induced  
214 with aspartate, cells induced with arginine, proline and ornithine had increased levels of activated  
215 Ras1 in its GTP bound form. We attempted to directly assess the requirement of adenylyl  
216 cyclase, however, the previously characterized *cdc35Δ/Δ* (*cyr1*) strain [26] did not grow in the  
217 synthetic media used here, even when the media was supplemented with 100 μg/ml uridine  
218 and/or 10 mM dibutyryl cAMP (data not shown). The lack of growth of this strain, which was  
219 contrary to our expectations, precluded a direct assessment of the role of Cyr1.

220 We tested whether amino acid catabolism was required to activate PKA-signaling by  
221 examining the morphology of colonies from cells grown on medium containing arginine or  
222 proline as sole nitrogen source and supplemented with enzyme specific inhibitors. In *C. albicans*,  
223 arginine is primarily catabolized via the arginase (*CARI*) pathway commencing with the  
224 hydrolysis of arginine to ornithine and urea. N<sup>ω</sup>-hydroxy-nor-arginine (Nor-NOHA), a potent  
225 competitive inhibitor of arginase [41], clearly inhibited arginine-induced filamentation in a dose-  
226 dependent manner (**Fig. 2D**). Similarly, L-tetrahydrofuroic acid (L-THFA), a specific  
227 competitive inhibitor of proline dehydrogenase (Put1)[42, 43], greatly impaired filamentation in  
228 a dose-dependent manner (**Fig. 2E**). The data demonstrate that the arginine- and proline-inducing  
229 signals are derived from their catabolism.

### 230 **Increased ATP resulting from mitochondrial metabolism of morphogenic amino acids** 231 **activate Ras1/cAMP/PKA signaling**

232 Intracellular levels of ATP are thought to provide a key input for Ras1/cAMP/PKA signaling  
233 [14]. Consistent with this notion, in comparison to cells grown in the presence of non-inducing  
234 nitrogen sources, such as aspartate and ammonium sulfate, cells grown in the presence of the  
235 morphogenic amino acids arginine, ornithine or proline contained similar, and significantly  
236 higher levels of ATP (**Fig. 3A**). Urea robustly induces filamentous growth, however, urea-  
237 derived signals bypass Ras1; morphogenic induction is dependent on *DURI,2*-dependent  
238 metabolism that generates CO<sub>2</sub> [30]. Interestingly, cells grown on media with urea, contained  
239 significantly lower levels of ATP.

240 Arginine and ornithine are catabolized to proline in the cytoplasm, and proline is subsequently  
241 metabolized to glutamate and then  $\alpha$ -ketoglutarate in the mitochondria [12]. These metabolic  
242 events generate the reduced electron donors, FADH<sub>2</sub> and NADH, which are oxidized by the  
243 mitochondrial electron transfer chain leading to ATP synthesis (**Fig. 3A**). We posited that the  
244 increased levels of ATP resulting from the catabolism of arginine, ornithine and proline is the  
245 consequence of their shared metabolic pathway. To test this, we used methylene blue (MB),  
246 which uncouples electron transport from the generation of a proton motive force across the inner  
247 mitochondrial membrane. The inclusion of MB in media containing ornithine or proline  
248 completely inhibited filamentous growth (**Fig. 3B**). Interestingly, the inhibitory effect of MB in  
249 cells growing on arginine was not complete, and a higher concentration of MB was required to  
250 noticeably inhibit filamentation. These latter findings suggest that an alternative arginine-  
251 induced pathway that is independent of ATP-generating mitochondrial metabolism exists in *C.*  
252 *albicans*.

253 We sought independent means to assess levels of reduced electron donors generated by the  
254 metabolism of the morphogenic amino acids. The membrane-permeable redox indicator TTC  
255 (2,3,5 triphenyltetrazolium chloride, colorless) is converted to TTF (1,3,5-triphenylformazan,  
256 red) in the presence of NADH and has been used to monitor mitochondrial respiratory activity  
257 of colonies [15, 44]. Colonies growing on proline, arginine, and ornithine exhibited a more  
258 intense, deep red pigment than colonies growing on aspartate (**Fig. S4, top panel**). The redox-  
259 sensitive dye resazurin can be used in liquid culture to monitor the reducing capacity of the  
260 intracellular environment [45]; resazurin is non-fluorescent, but is readily reduced by NADH or  
261 to a lesser extent by NADPH to highly red fluorescent resorufin (excitation 560 nm, emission  
262 590 nm). Consistent with the results obtained using TTC, cells growing with proline, arginine,  
263 or ornithine as sole nitrogen source exhibited 6 – 8-fold more resorufin fluorescence than  
264 aspartate grown cells (**Fig. S4, bottom panel**). These results indicate that cells grown in the  
265 presence of proline as the sole nitrogen source have a reducing intracellular environment, a  
266 finding aligned with the previous report by Land et al. [11].

267

268 **Proline metabolism generates the primary signal for arginine-induced morphogenesis**

269 Arginine is degraded in a pathway that bifurcates after the initial reaction catalyzed by Car1,  
270 which forms ornithine and urea (**Fig. 4A**). Ornithine is subsequently metabolized by ornithine  
271 aminotransferase (*CAR2*) to form glutamate  $\gamma$ -semialdehyde, which spontaneously converts to  
272  $\Delta^1$ -pyrroline-5-carboxylate (P5C). P5C is converted to proline by the *PRO3* gene product.  
273 Cytoplasmic proline is transported into the mitochondria where it is converted back to P5C by  
274 proline oxidase (*PUT1*). Finally, the mitochondrial P5C is converted to glutamate by the *PUT2*  
275 gene product (Marczak and Brandriss, 1989; Siddiqui and Brandriss, 1989), which is then  
276 converted to  $\alpha$ -ketoglutarate via Gdh2. Urea is further catabolized in the cytosol by urea  
277 amidolyase (*DUR1,2*) forming  $\text{NH}_3$  and  $\text{CO}_2$ .

278 Based on our results demonstrating that the filament-inducing effect of ornithine and proline  
279 requires mitochondrial respiration, we investigated if both branches of the bifurcated arginine  
280 degradative pathway could independently trigger filamentous growth. To accomplish this, we  
281 used a CRISPR/Cas9 strategy to construct PMRCA18-derived strains individually lacking *CAR1*  
282 (**Fig. S3D**), *DUR1,2* (**Fig. S3E**), or *PUT1*, *PUT2* and *PUT3* (**Fig. S3F**), or both *PUT1* and  
283 *DUR1,2* (**Fig. S3G**). Growth-based assays, on solid and in liquid media, confirmed that the *car1*-  
284 *-* strain exhibited impaired growth on synthetic glucose medium (**SXD**) containing arginine as  
285 a sole nitrogen source, whereas the strain grew like wildtype (WT) on **SXD** medium containing  
286 either 10 mM ornithine, proline or urea (**Fig. 4B and Fig. S5**). As expected, and similar to  
287 previous reports [30], the *dur1,2*-*-* strain exhibited severely impaired growth on medium  
288 containing urea as sole nitrogen source, but grew well in media containing arginine, ornithine or  
289 proline as sole nitrogen sources (**Fig. 4B and Fig. S5**). Cells lacking the proline oxidase (*put1*-  
290 *-*) were able to grow in media containing arginine, but unable to grow when ornithine or proline  
291 were the sole source of nitrogen (**Fig. 4B and Fig. S5**), indicating that ornithine utilization is  
292 strictly dependent on the mitochondrial proline catabolic pathway (**Fig. 4B and Fig. S5**).

293 Interestingly, and quite surprisingly, the *put1*-*- dur1,2*-*-* double mutant strain retained the  
294 ability to grow with arginine as sole nitrogen source, albeit slower, clearly suggesting that an  
295 arginase-independent arginine utilization pathway exists in *C. albicans* (**Fig. 4B and Fig. S5**).  
296 In subsequent growth-based assays the *car1*-*-* strain exhibited glucose-dependent growth  
297 phenotypes. The *car1*-*-* strain did not grow when arginine was present as the sole nitrogen and

298 carbon source, and in the absence of glucose, the *car1*<sup>-/-</sup> strain did not alkalinize the media (**Fig.**  
299 **S6**). Thus, in the presence of high glucose, the arginase-independent pathway merely enables the  
300 use of arginine as a nitrogen source.

301 Next we analyzed the expression of genes involved in arginine catabolism in cells after  
302 shifting them to minimal medium containing 10 mM arginine (YNB+Arg) as sole nitrogen and  
303 carbon source (**Fig. 4C**). One hour after the shift, the proline catabolic genes *PUT1* and *PUT2*  
304 were significantly upregulated. The levels of *PUT3*, the proline activated transcription factor that  
305 is constitutively bound to the promoter of *PUT1* and *PUT2*, did not change [46]. Strikingly,  
306 *DUR1,2* gene expression remained constant. Contrary to the assumption that Dur1,2 is  
307 responsible for alkalization of the medium, the consequence of the deamination of arginine-  
308 derived urea [47], we observed that the *dur1,2*<sup>-/-</sup> mutant still alkalinized the medium (**Fig. 4D**).  
309 Notably, both *put1*<sup>-/-</sup> and *put2*<sup>-/-</sup> strains failed to grow in this medium (**Fig. 4D**), indicating that  
310 the proline catabolic pathway branch of arginine utilization is essential for growth when arginine  
311 is both carbon and nitrogen source. Accordingly, an increased flux through the proline branch of  
312 the pathway and subsequent deamination of glutamate provides the likely explanation for the  
313 alkalization of the medium (**Fig. 4A**).

314 Consistent with their ability to support growth, arginine, ornithine and proline induced the  
315 expression of HA epitope-tagged Put2 (Put2-HA) (**Fig. 4E**). The induction was rapid, 1 h  
316 following the shift from YPD to SXD (X = 10 mM Asp, Arg, Orn or Pro), Put2 expression was  
317 derepressed in the presence of arginine and ornithine, almost to the levels observed by the  
318 addition of proline. Aspartate did not induce Put2 expression. Together these results indicate that  
319 arginine and ornithine are efficiently metabolized to proline, and metabolism associated with  
320 proline branch is required for the use of these amino acids as energy sources for growth.

321 To test whether proline catabolism is required for arginine-induced morphogenesis, we tested  
322 first whether morphogenesis in the presence of arginine can be reduced by Put1 inhibitor, L-  
323 THFA (Zhu et al., 2002; Zhang et al., 2015). As expected, pharmacological inhibition of Put1  
324 by L-THFA inhibited arginine-induced morphogenesis (**Fig. 4F**). We then carried out a genetic  
325 analysis to dissect the pathway triggering filamentous growth in the presence of arginine.  
326 Consistent with the existing model for arginine-induced morphogenesis [30], the *car1*<sup>-/-</sup> strain

327 formed extensively wrinkled colonies in the presence of 10 mM urea comprised mainly of  
328 filamentous cells (**Fig. 4G**). However, in comparison to wildtype colonies growing on arginine  
329 media, wrinkling was delayed and was first noticeable after 48 h of incubation. On media with  
330 an equimolar amount of arginine and urea (Arg + Urea) the *car1*<sup>-/-</sup> strain developed wrinkled  
331 colonies clearly visible after only 24 h. These findings suggest that arginine metabolism via the  
332 proline branch induces filamentation more rapidly than the CO<sub>2</sub> (HCO<sub>3</sub><sup>-</sup>) generated by the  
333 Dur1,2-dependent degradation of urea. Consistent with this notion, colonies formed by the *put1*<sup>-/-</sup>  
334 mutant remained relatively smooth even after 48 h of growth (**Fig. 4G**). In summary, our  
335 results indicate that the metabolism associated with proline branch of the arginine degradation  
336 pathway generates the primary and most rapid signal of arginine-induced morphogenesis.

337

### 338 **Proline utilization is sensitive to carbon source availability and independent of NCR** 339 **control**

340 The capacity of proline to stimulate filamentous growth is significantly affected by glucose  
341 availability (**Fig. 5A**). In comparison to colonies formed on synthetic media with 10 mM proline  
342 containing 2% glucose (SPD), colonies on media containing 0.2% glucose (SPD<sub>0.2%</sub>) exhibited  
343 larger feathery zones of hyphal cells emanating around their periphery. These findings are  
344 reminiscent of reports that *C. albicans* cells grown on media with methionine as nitrogen source  
345 and low glucose exhibit robust filamentation [31]. We considered the possibility that glucose  
346 repression of mitochondrial function, known to occur in *Saccharomyces cerevisiae* [48, 49], may  
347 underlie the difference. Consistent with this notion, macrocolonies formed on SPD were deeper  
348 red in color when overlaid with TTC than macrocolonies formed on SPD<sub>0.2%</sub> or on media with  
349 1% glycerol (SPG). The lighter red color of macrocolonies on low glucose, or on glycerol,  
350 confirm that cells have lower intracellular levels of NADH, i.e., under derepressing conditions  
351 when mitochondria can efficiently oxidize NADH (**Fig. 5A**).

352 We tested the notion that at low glucose concentrations, i.e., non-repressing conditions, cells  
353 use proline as a carbon source. Proline utilization was assayed directly by measuring the amount  
354 of residual proline in culture supernatants after a 2 h incubation period. In media containing 2%

355 glucose, cells took up < 2% of the proline. By contrast, cells growing in low glucose (0.2%) or  
356 1% glycerol used 12 – 15% of the available proline (**Fig. 5B**). The expression of Put2 was  
357 independent of glucose, as the levels of Put2 were similar (**Fig. 5B, insert**). These results indicate  
358 that proline is taken up and metabolized more efficiently in cells under non-repressing  
359 conditions, suggesting that mitochondrial activity is subject to glucose repression.

360 To critically test this, we assessed the effect of varying the glucose concentration from 0.05 -  
361 4%. Cells were grown for 16 h in media containing the pH indicator bromcresol purple. At high  
362 glucose concentrations (0.5 – 4%) the media remained acidic, indicating cells were growing  
363 fermentatively using proline merely as a nitrogen source (**Fig. 5C**). By contrast, at glucose  
364 concentrations  $\leq 0.2\%$ , the media became alkaline, indicating that cells were respiring and using  
365 proline as the primary energy source. The increased flux through the proline pathway is expected  
366 to yield elevated  $\text{NH}_3$  generated by the mitochondrial glutamate dehydrogenase (*GDH2*)  
367 catalyzed deamination of glutamate. To directly assess mitochondrial activity under these  
368 conditions, we carried out extracellular oxygen consumption analysis in a high-throughput  
369 microplate format (**Fig. S7**). Cells grown in repressing  $\text{SPD}$  had the lowest oxygen consumption  
370 whereas those grown at  $\text{SPD}_{0.2\%}$  had the highest, higher than cells grown in  $\text{SPG}$ . As previously  
371 pointed out, Put2 levels were similar across all conditions (**Fig. 5B**). Together, these results  
372 indicate that proline is taken up and then metabolized more efficiently in cells growing under  
373 low glucose concentrations. Consistent with this finding, Put2 expression was derepressed in  
374 rich media containing yeast extract and peptone when non-repressing, non-fermentative carbon  
375 sources replaced glucose; i.e., glycerol or lactate (**Fig. 5D**). Similarly, cells express elevated  
376 levels of Put2 when grown in hyphal inducing Spider medium, a medium rich in amino acids  
377 and mannitol as a primary carbon source.

378 Nitrogen regulation of transcription in fungi is a suprapathway response that is commonly  
379 referred to as nitrogen catabolite repression (NCR), which functions to ensure that cells  
380 selectively use preferred nitrogen sources when available. Briefly, NCR regulates the activity of  
381 GATA transcription factors Gln3 and Gat1; in the presence of preferred nitrogen sources, these  
382 factors do not gain access to the promoters of NCR-regulated genes (reviewed in[50]). Previous  
383 studies have shown that certain amino acids, traditionally classified as poor (e.g., proline) in *S.*

384 *cerevisiae*, were readily utilized by *C. albicans* mutants lacking Gln3 and Gat1 [51]; the  
385 introduction of null alleles of both *GLN3* and *GAT1* in *C. albicans* did not impair growth using  
386 proline as sole nitrogen source, whereas growth on urea was severely affected. Consistent with  
387 these findings, we found that Put2-HA was constitutively expressed in *gln3Δ/Δ gat1Δ/Δ* mutant  
388 grown in medium containing high levels of the preferred nitrogen source ammonium sulfate  
389 (**Fig. 5E**). Our data indicate that in *C. albicans* proline utilization is not subject to NCR, a  
390 conclusion aligned with recently published transcriptome analyses[46].

391

### 392 **Proline induces hyphal growth within phagosomes and enables *C. albicans* to escape from** 393 **engulfing macrophages**

394 We sought to place our novel insights regarding the critical role of proline metabolism in the  
395 induction of hyphal growth in a broader biological context and tested whether proline catabolism  
396 affects the capacity of *C. albicans* cells to form hyphae within macrophages and escape killing.  
397 First, using indirect immunofluorescence microscopy we examined whether Put2-HA is  
398 expressed in *C. albicans* cells engulfed by murine RAW264.7 macrophages (**Fig. 6A**). *C.*  
399 *albicans* CFG185 (*PUT2/PUT2-HA*) cells were co-cultured with macrophages (MOI of 5:1;  
400 C:M) for 90 min. Strain CFG185 exhibits activation of proline catabolism in the presence of  
401 arginine, ornithine, and proline (**Fig. 4E**). The macrophages were imaged using antibodies  
402 against the HA tag (1<sup>o</sup>, rat anti-HA; 2<sup>o</sup>, goat anti-rat antibody conjugated to Alexa Fluor 555)  
403 and LAMP-1, a lysosomal marker that is enriched in phagosomes. Confocal images clearly  
404 showed that *C. albicans* cells engulfed by macrophages express Put2, and that the Put2  
405 expressing fungal cells localized to Lamp1 compartments (see the orthogonal view of merged  
406 channels, lower left panel). The results indicate that *C. albicans* cells within macrophage  
407 phagosomes express Put2.

408 Next, we assessed the importance of the proline catabolic pathway components in the capacity  
409 to escape macrophage. To facilitate comparisons with results obtained in other laboratories, we  
410 repeated the construction of the proline catabolic pathway mutations in the SC5314 strain  
411 background; strains lacking *PUT1*, *PUT2*, *PUT3* or both *PUT1* and *PUT2* were constructed using

412 CRISPR/Cas9. The full genome of each mutant strain was sequenced; the sequence coverage  
413 varied from 42 – 65X and after assembly the contig coverage accounted for  $\geq 98$  of the reference  
414 SC5314 genome (Assembly 22, version s06-m01-r01; [52]). Each strain was found to carry the  
415 intended null mutation in the correct chromosomal locus and no large scale dissimilarities to the  
416 reference genome or off-target mutations were evident. Furthermore, no phenotypic differences  
417 were detected in comparison to the PMRCA18-derived strains (data not shown).

418 As expected, SC5314 (WT) and CRISPR/Cas9 control strains (pV1093 and pV1524), lacking  
419 guide sequences to target Cas9, exhibited robust hyphal growth when co-cultured with  
420 RAW264.7 macrophages (**Fig. 6B**). By contrast, and similar to heat killed SC5314, the strains  
421 carrying *put1*<sup>-/-</sup>, *put2*<sup>-/-</sup>, *put3*<sup>-/-</sup> and *put1*<sup>-/-</sup> *put2*<sup>-/-</sup> mutations were unable to efficiently form  
422 filaments from within engulfing macrophages (**Fig. 6B**). As hyphal formation enables *C.*  
423 *albicans* cells to escape macrophages and thereby facilitates survival, we analyzed the  
424 candidacidal activity of macrophages by assessing fungal cell viability by assessing colony  
425 forming units (CFU). Consistent with our microscopic analysis, in comparison to wildtype cells,  
426 the proline mutants were killed more efficiently (**Fig. 6C**). Together, these results indicate that  
427 *C. albicans* cells rely on proline catabolism to induce hyphal growth in phagosomes, a response  
428 that facilitates escape from killing by macrophages.

429  
430

## 431 **Discussion**

432 In this study we have found that ATP generating mitochondrial proline catabolism is required to  
433 induce hyphal development of *C. albicans* cells in phagosomes of engulfing macrophages. The  
434 finding that proline catabolism, also required for the utilization of arginine and ornithine, is  
435 required to sustain the energy demands of hyphal growth provides the basis to understand the  
436 central role of mitochondria in fungal virulence. The energy status of the fungal cell is clearly a  
437 key signal that engages the genetic programs underlying yeast-to-hyphal transitions. The  
438 dependence on the energy producing proline catabolic pathway to induce *C. albicans* cells to  
439 switch morphologies is instrumental in their ability to escape from macrophages. Our results are  
440 consistent with a recent model postulating that elevated cellular levels of ATP induces hyphal

441 morphogenesis [14] and with early reports that amino acid catabolism promotes filamentous  
442 growth [12, 13, 53]. Our experimental findings are schematically summarized in Fig. 7.

443 Our work provides a framework to integrate several fragmentary observations regarding  
444 amino acid-induced morphogenesis. For example, Land et al. [11, 12] observed that the most  
445 potent morphogenic amino acids arginine and proline are those metabolized to glutamate. Our  
446 results show that this occurs strictly via the mitochondrial localized proline utilization pathway  
447 essentially as described in *S. cerevisiae* [54-56] with the exception that proline metabolism is  
448 not under nitrogen regulation (**Fig. 5E**, [46]). Consistently, ornithine, an intermediate in arginine  
449 catabolism, also acts as a potent inducer of morphogenesis (**Fig. 1A**; [12, 53]). Glutamate is  
450 further converted to  $\alpha$ -ketoglutarate, an intermediate in the TCA cycle. These metabolic  
451 reactions are coupled to the generation of reduced electron carriers FADH<sub>2</sub> and NADH, which  
452 are oxidized in the mitochondria powering ATP synthesis. Amino acid induction of hyphal  
453 growth exhibits a strict requirement for Ras1 (**Fig. 2B**) and cells grown in the presence of these  
454 inducing amino acids have high levels of active Ras1 (**Fig. 2C**) and elevated levels of  
455 intracellular ATP (**Fig. 3A**). The metabolic inhibitors nor-NOHA (Car1) and L-THFA (Put1)  
456 and the mitochondrial uncoupler methylene blue (MB) block the induction of filamentation (**Fig.**  
457 **2D, E** and **Fig. 3B**). Our analysis demonstrates that arginine and proline induce morphogenesis  
458 by virtue of a shared metabolic pathway (**Fig. 4C-F**).

459 Together, our findings are well aligned to the recent model proposed by Grahl et al. [14],  
460 where mitochondrial ATP synthesis facilitates Ras1 activation in cooperation with the adenylyl  
461 cyclase (Cyr1) leading to increased cAMP production and to activation of the Efg1 transcription  
462 factor. The finding that arginine-induced hyphal growth occurs rapidly (**Fig. 4G**), suggests that  
463 a brief exposure to arginine may suffice to trigger filamentous growth. According to Grahl et al.  
464 (2015), Ras1 activation by ATP appears to be independent of the AMP kinase, a key regulator  
465 of cellular energy homeostasis. The ATP-binding pocket within the active site of mammalian  
466 adenylyl cyclase has been shown to act as an ATP sensor [57]. Although it has been proposed  
467 that Cyr1 may function similarly as an ATP sensor this has yet to be confirmed in *C. albicans*.  
468 Regardless of the mechanism, exceeding a critical threshold of ATP is likely required to induce  
469 cAMP synthesis. It is known that the cAMP produced by Cyr1 does not necessarily correlate to

470 the strength of the inducer and that transient short-lived spikes in cAMP are sufficient to trigger  
471 phosphorylation and eventually activation of Efg1 [27]. Consequently, spikes of ATP transiently  
472 generated by proline catabolism may efficiently induce hyphal specific genes (*HSG*).

473 We have clearly shown that arginine-, ornithine- and proline-induced hyphal growth is  
474 dependent on Ras1, which is not accounted for by other models of amino acid-induced  
475 morphogenesis (reviewed in [4, 7], despite the fact that Ras1 is known to be important in  
476 induction of filamentous growth in the presence of amino acid-rich serum [22]. Both the  
477 presumed amino acid sensitive Gpr1-Gpa2 pathway [58, 59] and the Dur1,2-dependent CO<sub>2</sub>  
478 model for arginine-induced morphogenesis [30] are thought to bypass Ras1 and involve direct  
479 interactions with adenylyl cyclase (*Cyr1*). Also, contrary to the previous report [30], CO<sub>2</sub>  
480 generated by the Dur1,2-dependent catabolism of urea is not the primary morphogenic signal.  
481 Specifically, induction of filamentous growth in the presence of arginine or proline as sole  
482 nitrogen source proceeds more quickly than that observed by the metabolism of urea (**Fig. 4G**).  
483 In addition, *DURI,2* expression is tightly regulated by NCR, i.e., in the presence of ammonia,  
484 urea metabolism is repressed [51]. By contrast, the conversion of arginine to proline is not under  
485 NCR control (**Fig. 5E**, [46]). Finally, when cells were shifted from YPD to medium containing  
486 arginine as sole carbon and nitrogen source, proline catabolic genes (*PUT1* and *PUT2*) were  
487 derepressed much faster than *DURI,2* (**Fig. 4C**), indicating that arginine is rapidly converted to  
488 proline. We have noted that the constitutive expression of arginase represents a common and  
489 undesired technical problem in proteomic analyses using SILAC (Stable Isotope Labeling  
490 by/with Amino acids in Cell culture) due to the rapid conversion of arginine to proline in  
491 eukaryotes [60-63]. In *Schizosaccharomyces pombe*, the deletion of two arginase genes (one a  
492 *CAR1* homologue) and the single ornithine transaminase (*CAR2* homologue) rectified this  
493 problem [60]. We predict, that similar deletions would be helpful in the quantitative analysis of  
494 the *C. albicans* proteome.

495 Earlier reports by Nickerson and Edwards [64] and Land et al. [11] suggested that  
496 mitochondrial activity is repressed during filamentous growth. By contrast, other more recent  
497 work has shown that hyphal formation occurs predominantly under aerobic conditions [16] and  
498 is associated with increased respiratory activity [14, 15]. Based on our findings (**Fig. 5C**), the

499 seemingly conflicting observations could be explained if, as in *S. cerevisiae*, the synthesis of  
500 mitochondrial respiratory enzymes are subject to glucose repression [65, 66]. There is  
501 surprisingly little information available regarding glucose repression of mitochondrial function  
502 in *C. albicans*, and whether the regulatory circuits are wired similar to those in *S. cerevisiae*.  
503 However, we note that Land et al. [11] used growth conditions with high glucose (~1.8%; 100  
504 mM), whereas studies by [14, 15] were carried out using low glucose (10 mM, i.e., ≈ 0.2% ).

505 In striking contrast to the current view that *C. albicans* mitochondrial function is insensitive  
506 to glucose repression [67-69], our results clearly demonstrate that glucose represses respiration  
507 in the presence of proline (**Fig. S7**). Cells grown aerobically in high glucose exhibit fermentative  
508 metabolism (**Fig. 5C**), i.e., the well-characterized Crabtree effect [70]. In glycolysis, conversion  
509 of glucose to pyruvate is coupled to reduction of NAD<sup>+</sup> and to the generation of ATP. Only small  
510 amounts of the cofactor is available in the cytosol. Consequently, when mitochondrial functions  
511 are glucose repressed, cells use fermentation to oxidize NADH and regenerate NAD<sup>+</sup>, thereby  
512 enabling cytoplasmic ATP synthesis to continue. Under conditions when proline is the sole  
513 nitrogen source and high glucose is present, cells use glucose for energy and as carbon-source,  
514 whereas proline catabolism merely supplies cells with nitrogen, i.e., proline utilization is low  
515 (**Fig. 5B**). However, when glucose becomes limiting (<0.2%), the respiratory capacity of  
516 mitochondria increases (**Fig. S7**), enabling cells to efficiently oxidize NADH and generate ATP  
517 by oxidative phosphorylation; under these conditions cells use proline for energy and as the  
518 carbon- and nitrogen-source, i.e., proline utilization is high (**Fig. 5B**). Together our results show  
519 that proline metabolism is a sensitive indicator of mitochondrial function in *C. albicans*.

520 Our observation that high glucose represses mitochondrial function, provides a mechanistic  
521 understanding of how high glucose inhibits hyphal morphogenesis [13, 31]. Cells grown on 2%  
522 glucose have elevated levels of reduced cofactors, such as NADH (**Fig. 5A**), suggesting that the  
523 capacity of mitochondria to oxidize NADH is suboptimal, i.e., the cellular capacity to regenerate  
524 NAD<sup>+</sup> is rate limiting, a phenomenon termed over-flow metabolism [48]. It is important to note  
525 that, based on the *S. cerevisiae* paradigm, the pyruvate formed in glycolysis needs to be  
526 converted to acetyl-CoA to prime the TCA cycle. The mitochondrial-localized pyruvate

527 dehydrogenase complex is predominantly responsible for the conversion of pyruvate to acetyl-  
528 CoA during glucose-limited, respiratory growth [65, 66]. Indeed, pharmacological inhibition of  
529 glycolysis has been shown to arrest filamentous growth of *C. albicans* even in the presence of  
530 proline [11]. Alternatively,  $\beta$ -oxidation of lipids may contribute the necessary acetyl-CoA [9].

531 We have placed the SPS sensing pathway, the primary sensing system of extracellular amino  
532 acids, in context to the major intracellular signaling pathways governing in nutrient regulated  
533 morphogenesis. SPS-sensor initiated signals do not directly induce hyphal growth, but rather  
534 facilitate morphogenesis by up-regulating the capacity of cells to take up inducing amino acids  
535 (Fig. 7). Experimental support for this conclusion includes the following observations. First,  
536 amino acid-induced activation of SPS-sensor signaling does not strictly correlate with the  
537 induction of filamentous growth (Fig. 1A). Second, the inability of a *ssy1* null mutant to undergo  
538 morphogenesis can be rescued by expressing a constitutively active form of Stp2 (*STP2\**) but  
539 not Stp1 (*STP1\**). Stp2 is the effector transcription factor that controls amino acid permease gene  
540 expression, whereas Stp1 activates the expression of secreted aspartyl proteases and oligopeptide  
541 transporters [34]. Consistently, and similar to Kraidlova et al. [71], we found that the expression  
542 of six *C. albicans* orthologues (*GAP1-GAP6*) of the *S. cerevisiae* general amino acid permease  
543 (*GAP1*) are regulated by the SPS sensing system, perhaps with the exception of *GAP4*  
544 expression, which is comparatively expressed at very low levels (data not shown). Third,  
545 filamentous growth is dependent on amino acid catabolism. The weak filamentation observed in  
546 the *csH3* $\Delta/\Delta$  mutant grown in 10 mM proline can be attributed to the residual uptake of proline  
547 as previously described [35]; apparently, the residual systems are expressed and function at high  
548 extracellular concentrations of proline [53, 72]. Thus, the filamentous growth defect observed in  
549 cells lacking a functional SPS sensing pathway, i.e., *SSY1* or *CSH3* null mutants, is due to the  
550 inability to efficiently take up inducing amino acids from the extracellular environment, a  
551 requisite for their metabolism [35, 36].

552 Together our findings have important implications on understanding how *C. albicans* cells  
553 interact with host immune cells. Transcriptomic studies examining macrophage-*C. albicans*  
554 interactions by Lorenz et al. [9] showed that arginine biosynthesis genes are peculiarly  
555 upregulated in phagocytosed cells. Furthermore, the results suggest that the phagosome is likely

556 a glucose-poor environment as an increased expression of genes that favor gluconeogenesis and  
557 mitochondrial function was also noted [9]. Interestingly, arginine utilization appears to proceed  
558 concomitant with arginine biosynthesis as deduced from the increased arginase transcripts in  
559 phagocytosed cells [9, 30]. In a follow-up study, the apparent upregulation of arginine  
560 biosynthesis was suggested to be a response to the macrophage oxidative burst [73].  
561 Interestingly, the expression of *DUR1,2* in phagocytosed cells was not significantly altered. Our  
562 finding that the enzymes responsible for proline utilization are upregulated indicates that proline  
563 is either made available by the host or is the result of arginine catabolism.

564 In the light of these results, the challenging question is where the hyphae inducing amino  
565 acids come from, from the macrophage or from nutrients stored within *C. albicans* cells prior to  
566 their being phagocytosed. In *S. cerevisiae*, > 90% of free arginine is sequestered in the vacuole  
567 and the non-compartmentalized and cytosolic arginine is catabolized by arginase [74]. Given  
568 that arginine is catabolized to proline via the arginase pathway with ornithine acting as a  
569 transitory intermediate, it is possible that vacuolar stores of arginine are activated in the  
570 phagosome to support the demand for cellular energy. When glucose becomes limiting, *C.*  
571 *albicans* may rely on the catabolism of amino acids, particularly proline, as primary energy. This  
572 is reminiscent of the requirement of proline catabolism for Trypanosome survival in the Tsetse  
573 fly vector [75-78].

574 Proline-induced morphogenesis is repressed under acidic conditions [13, 53], presumably a  
575 condition confronting newly phagocytized *C. albicans* cells. This raises the interesting  
576 conundrum as to how *C. albicans* cells deal with this environmental challenge and filament. It  
577 is possible that Stp2-mediated alkalization of the phagosome reported by Vylkova and Lorentz  
578 [79] is a key predisposing event that facilitates proline-induced morphogenesis. We found that  
579 alkalization is not Dur1,2-dependent (**Fig. 4D**), indicating that an alternative mechanism triggers  
580 alkalization. Accordingly, the Stp2-dependent induction of arginine uptake and its subsequent  
581 Put1- and Put2-dependent metabolism generates glutamate, which is deaminated to  $\alpha$ -  
582 ketoglutarate by glutamate dehydrogenase (Gdh2) (**Fig. 7**). The resulting NH<sub>3</sub> may provide the  
583 explanation for the observed alkalization. As already pointed out, the source of amino acids in  
584 the macrophage phagosome remains a very interesting question. Numerous metabolic signatures

585 appear to reflect a microenvironment with a poor nitrogen content. For example, based on the  
586 transcriptional analysis of the *C. albicans*-macrophage interaction, *OPT1*, encoding an  
587 oligopeptide transporter, is upregulated in phagocytosed cells [9]. *OPT1* expression is controlled  
588 by the SPS-sensor signaling and the downstream transcription factor Stp1 [34, 37]. *STP1*  
589 expression is itself under tight NCR control [37]. Thus, the upregulated expression of *OPT1*  
590 strongly suggests that NCR is relieved in phagocytosed cells and that sufficient levels of amino  
591 acids are present to induce the SPS-sensor. As to the origin of amino acids in the phagosome, *C.*  
592 *albicans* may excrete amino acids liberated from storage compartments, loaded during growth  
593 in rich media. In *S. cerevisiae*, under defined conditions, amino acids are known to be excreted  
594 at detectable levels [80] and under certain circumstances activate SPS-sensor signaling [81].  
595 Thus, amino acids may provide an autocrine function to induce filamentous growth of  
596 phagocytosed *C. albicans* cells.

597 The results presented here provide a clear example of how *C. albicans* cells sense and respond  
598 to nutrients present in the host to ensure proper nutrient uptake and continued survival. The  
599 molecular components underlying nutrient uptake are often referred to as virulence factors.  
600 When afforded the opportunity, *C. albicans* will alter developmental programs to optimize  
601 nutrient uptake systems that enable the better exploit host environments and to evade the primary  
602 immune response [3, 82, 83]. The identification and understanding of fungal virulence factors is  
603 necessary to therapeutically disturb their function upon infectious growth and thereby facilitate  
604 the ability of host immune systems to re-establish and maintain the integrity of the host. We are  
605 excited by the prospect of exploiting mitochondrial proline metabolism to probe the nutrient  
606 environment of the macrophage phagosome, a currently poorly characterized environment.

607

608

## 609 **Materials and methods**

### 610 **Strains, media and chemicals**

611 *C. albicans* strains are listed in Supplementary Information Table S1 and all primers used are  
612 listed in Table S2. All strains were cultivated in YPD medium (1% yeast extract, 2% peptone,

613 2% glucose) at 30 °C. Minimal synthetic dextrose (SD) medium containing 0.17% YNB (Yeast  
614 Nitrogen Base without amino acids and without ammonium sulfate; Difco™), 2% glucose, and  
615 5 g/l ammonium sulfate ( $\approx$  38 mM) was used as indicated. Media were made solid by 2% (w/v)  
616 Bacto agar. Where appropriate, 100 or 200  $\mu$ g/ml nourseothricin (Nou; Jena Biosciences, Jena,  
617 Germany) was added to the medium. The ability of amino acids to induce filamentous growth  
618 was determined on buffered solid synthetic (SXD) media containing 0.17% YNB, 2% glucose,  
619 and 10 mM of the indicated amino acid (X) as sole nitrogen source, or at concentrations as  
620 described in the figure legends. Fifty mM 2-(N-morpholino) ethanesulfonic acid (MES) was  
621 included in media and the pH was adjusted to 6.0 using NaOH. To minimize residual nitrogen,  
622 the SXD media were made solid using 2% (w/v) highly purified agar (Biolife, Milano, Italy).  
623 Where indicated 0.2% glucose, 1% lactate or 1% glycerol replaced 2% glucose as carbon source.  
624 The following media were used to screen CRISPR/Cas9-derived knockout phenotypes: YPD-  
625 MM; SUD; SPD; and YNB+Arg+BCP. YPD-MM is standard YPD supplemented with 1.5  
626 mg/ml MM (2-((((4-methoxy-6-methyl)-1,3,5-triazin-2-yl]-amino)carbonyl)amino]-sulfonyl)-  
627 benzoic acid; Dupont™ Ally); SUD and SPD were prepared as SXD containing urea (U), or  
628 proline (P) as sole nitrogen source; YNB+Arg+BCP contains 0.17% YNB, 10 mM arginine  
629 (Arg) as sole nitrogen and carbon source, and 0.03  $\mu$ g/mL bromocresol purple (BCP; Sigma) as  
630 indicator, with the pH adjusted to 4.0 using 1 M HCl. Growth in the presence of specific  
631 metabolic inhibitors was assessed on media containing nor-NOHA (N-hydroxy-nor-L-arginine;  
632 BioNordika AB, Sweden) prepared in 100% dimethyl sulfoxide (DMSO) as 56 mM concentrated  
633 stock; a 26 mM working stock was prepared freshly diluting in ddH<sub>2</sub>O. L-tetrahydro-2-furoic  
634 acid (L-THFA; Sigma) and methylene blue (MB; Sigma), were freshly prepared in ddH<sub>2</sub>O as 1  
635 M and 3 mM stocks, respectively. *Escherichia coli* strain DH10B™ was used for the  
636 construction of plasmids; LB medium supplemented where required with carbenicillin (Cb, 50  
637  $\mu$ g/ml), Nou (50  $\mu$ g/ml), and/or chloramphenicol (Cm, 30  $\mu$ g/ml). LB was made solid by 1.5%  
638 Bacto agar. Liquid cultures were grown with agitation at 150-200 rpm. The density of yeast  
639 suspensions was determined and adjusted (1 OD<sub>600</sub> = 3 x 10<sup>7</sup> CFU/ml) [84]. Sterile Milli-Q™  
640 ddH<sub>2</sub>O was used in all experiments.

641

## 642 CRISPR/Cas9 mediated gene inactivation

643 The CRISPR/Cas9 gene editing was used to inactivate both alleles of *SSY1* (C2\_04060C), *CSH3*  
644 (C4\_03390W), *CARI* (C5\_04490C), *PUT1* (C5\_02600W), *DURI,2* (C1\_04660W), *IRA2*  
645 (C1\_12450C), *PUT1* (C5\_02600W), *PUT2* (C5\_04880C) or *PUT3* (C1\_07020C). Sequences of  
646 synthetic guide RNAs (sgRNAs), repair templates, and verification primers are listed in Table  
647 S2. The solo system plasmids pV1093 or pV1524 were used [85, 86]. These plasmids contain a  
648 cassette comprised of the *Candida/Saccharomyces* codon-optimized *CAS9* endonuclease gene,  
649 *NAT* gene (recyclable in pV1524), sgRNA cloning site, and flanking sequences for genomic  
650 integration. For pV1093 and its derivative plasmids, the cassettes were integrated in one of the  
651 *ENO1* loci, whereas pV1524 and its derivatives were integrated in one of the *NEUT5* loci. The  
652 sgRNAs were designed as described [87] and were inserted in pV1093 or pV1524 by linker  
653 ligation. To summarize, oligo pairs p43/p44 (*SSY1*), p49/p50 (*CSH3*), p55/p56 (*CARI*), p61/p62  
654 (*DURI,2*), p67/p68 (*IRA2*), p73/p74 (*PUT1*), p79/p80 (*PUT2*), and p85/p86 (*PUT3*), were  
655 separately phosphorylated and annealed prior to ligating them to dephosphorylated *Esp31*  
656 (*BsmBI*)-digested pV1093 or pV1524. Ligation reactions were purified and introduced into *E.*  
657 *coli* by electroporation. Transformants were selected on solid LB+Cb (or +Nou for pV1524  
658 cloning) incubated overnight at 37 °C. Plasmids were sequenced using primer p91 (FS95).  
659 Plasmids (3 to 6 µg) containing the 20-bp sgRNA for *SSY1* (pFS013), *CSH3* (pFS017), *CARI*  
660 (pFS024), *DURI,2* (pFS039), *IRA2* (pFS028), *PUT1* (pFS080, pV1093 derivative), *PUT1*  
661 (pFS088, pV1524 derivative), *PUT2* (pFS083) and *PUT3* (pFS084) were digested with *KpnI* and  
662 *SacI* to release the cassette. Repair templates (RT) containing stop codon and specific restriction  
663 site were produced by template-less PCR using oligo pairs p45/p46 (*SSY1*), p51/p52 (*CSH3*),  
664 p57/p58 (*CARI*), p63/p64 (*DURI,2*), p69/p70 (*IRA2*), p75/p76 (*PUT1*), p81/p82 (*PUT2*), and  
665 p87/p88 (*PUT3*). PCR-purified digested plasmid and repair templates were co-transformed into  
666 *C. albicans* cells at a 1:3 ratio (w/w, plasmid:repair template). The hybrid lithium acetate/DTT-  
667 electroporation method, with minor modifications, was used for transforming *C. albicans* [88].  
668 After applying 1.5 kV of electric pulse, cells were recovered in YPD medium supplemented with  
669 1 M sorbitol for at least 4 h and then plated on YPD+Nou plates; Nou<sup>R</sup> colonies were selected 2  
670 days after plating. Nou<sup>R</sup> transformants were pre-screened according to the expected phenotype

671 prior to PCR and restriction analysis using primers and restriction enzymes indicated in Table  
672 S2 (**Fig. S3**).

673

#### 674 **Full genome shotgun sequencing**

675 Genomic DNA was isolated from *put1*<sup>-/-</sup> (CFG139), *put2*<sup>-/-</sup> (CFG207), *put3*<sup>-/-</sup> (CFG146), *put1*<sup>-/-</sup>  
676 *put2*<sup>-/-</sup> (CFG159) and CRISPR/Cas9 control strains CFG181 (pV1093) and CFG182 (pV1524)  
677 and sequenced. Prior to library construction, extracted DNA was purified with Agencourt  
678 AMPure<sup>®</sup> XP beads (Beckman Coulter, USA) in order to remove short sequences (<100 bp).  
679 Aliquots (25 µl) of DNA were mixed with 45 µl of AMPure beads with a ratio of 1:1.8 and  
680 incubated 15 min. Initial DNA concentrations following purification were evaluated using  
681 Quant-iT PicoGreen dsDNA Assay kit (ThermoFisher, USA) as described (Logares & Feng,  
682 2010). Absorbance was measured at 530 nm, using a Tecan Ultra 384 SpectroFluorometer  
683 (PerkinElmer, USA).

684 Library construction was carried out with the QIAGEN-FX kit (Qiagen, Germany) with a  
685 DNA input of 100 ng DNA per sample and a digestion time of 13 min without enhancer.  
686 Following fragmentation, adapter sequences were ligated, and ligated DNA fragments were  
687 amplified by 9 cycles of PCR and DNA was purified with AMPure<sup>®</sup> XP beads. The quality of  
688 the library samples were evaluated with an Agilent Bioanalyzer using DNA1000 cartridges. The  
689 average length of the fragments excluding adapter sequences was 455 bp.

690 Prior to sequencing, the samples were denatured with 0.2 N NaOH. A final volume of 570  
691 µl of pooled library was mixed with denatured Phix control (30 µl) and loaded on an Illumina  
692 Mi-Seq 2x300 flow-cell and reagent cartridge. De-multiplexing and removal of indexes and  
693 primers were done with the Illumina software v. 2.6.2.1 on the instrument according to the  
694 standard Illumina protocol. Initial de novo assembly of quality controlled reads was done with  
695 SPADES v. 3.11.1 and standard settings [89]. Mapping of assembled contigs was done with  
696 Ragout v 2.0 [90] using Sibelia for synteny detection[91]. Visualization of results and generation  
697 of reports on the assembly quality and other factors were done with QUAST v. 4.6.1 [92].

698

699 **NanoLuc transcription-translation reporter of SPS-sensor activation**

700 The NanoLuc-PEST (Nlucp) construct was used to create the reporter of SPS-sensor dependent  
701 transcription (**Fig. S2**). The presence of PEST sequences ensures rapid degradation of NanoLuc  
702 luciferase, thereby enhancing sensitivity [39]. Up- and downstream regions of the *CAN1* ORF  
703 were amplified using genomic DNA from PMRCA18 as template and primers p92/p93 (0.9 kB  
704 upstream) and p96/p97 (0.98 kB downstream) (**Table S2**). An approximately 0.7 kB Nlucp gene  
705 sequence was amplified from plasmid pCA873 [93] using primers p94/p95. These amplicons  
706 were digested with appropriate FastDigest enzymes (Thermo Scientific) and purified; i.e., the  
707 *CAN1* upstream amplicon was digested with *KpnI/XhoI*, the *CAN1* downstream with *XbaI/NotI*,  
708 and Nlucp DNA fragment with *XhoI/BamHI*. Using T4 DNA Ligase (Thermo Scientific), the  
709 upstream fragment was first ligated to *KpnI/XhoI*-digested pSFS2a vector [88] creating pFS006.  
710 The purified Nlucp DNA was then ligated into *XhoI/BamHI* restricted pFS006 creating pFS007.  
711 Finally, the downstream fragment was ligated into *XbaI/NotI* restricted pFS007 creating pFS010.  
712 The plasmids were introduced into *E. coli* and transformants selected on LB+Cm+Nou plates  
713 incubated at 30 °C. The desired reporter construct, purified from *KpnI/NotI* restricted pFS010,  
714 was introduced into *C. albicans* wildtype (PMRCA18) and SPS-deficient mutant strains  
715 (*ssy1Δ/Δ*, *ssy5Δ/Δ*, and *stp2Δ/Δ*) by electroporation. Selection was carried out on YPD+Nou and  
716 NAT<sup>R</sup> clones carrying the integrated Nlucp construct were identified by PCR.

717 For analysis of amino acid-induced SPS-sensor activation, Nano-Glo<sup>®</sup> Luciferase Assay  
718 System (Promega GmbH, Germany) was used following the manufacturer's protocol. Briefly,  
719 log phase SD cultures were first standardized to OD  $\approx$  0.8 before adding 50  $\mu$ l of the cell  
720 suspension into each well of Nunc 96 well microplate (white). Then, cells were induced with 50  
721  $\mu$ M of the indicated amino acids for 2 h at 30 °C. Fifty microliters (50  $\mu$ l) of Nano-Glo substrate  
722 diluted 1:50 in the supplied lysis buffer was added into each well of the microplate. After 3 min,  
723 bioluminescence was captured using microplate luminometer (Orion II, Berthold Technologies  
724 GmbH & Co. KG, Germany). Luminescence reading from treated wells were deducted from  
725 wells spiked with ddH<sub>2</sub>O serving as uninduced control.

726

727 **Filamentation assay**

728 Solid filamentation assay was performed as described [14]. Briefly, cells from overnight YPD  
729 liquid cultures were harvested, washed once, and resuspended in sterile ddH<sub>2</sub>O. The cell density  
730 of cell suspensions was adjusted to OD<sub>600</sub> ≈ 8 before spotting 10 μl onto solid media. Plates were  
731 allowed to dry at room temperature before incubating at 37 °C as indicated to allow  
732 macrocolonies to form. Filamentation assays in the presence of metabolic inhibitors, nor-NOHA  
733 or L-THFA, were performed in a 6-well microplate format (~5 ml/well); otherwise, all assays  
734 were carried out using standard Petri plates (~35 ml/plate). For filamentation assays in liquid  
735 cultures, cells were washed and then adjusted to OD<sub>600</sub> ≈ 25. Cells were diluted in pre-warmed  
736 liquid medium at OD<sub>600</sub> ≈ 0.5 and then incubated at 37 °C with vigorous agitation for the  
737 specified time. Cell morphologies were assessed under epifluorescence microscopy using  
738 calcofluor white stain (CFW, Fluorescent Brightener 28, 1 mg/ml; Sigma).

739

740 **qRT-PCR**

741 Hyphal specific gene (HSG) expression in 24 h old macrocolonies was analyzed as follows:  
742 using a sterile glass slide, three to four macrocolonies of wildtype strain (PMRCA18) were  
743 collected by scraping and suspended in 1 ml of ice-cold PBS. Cells were harvested by  
744 centrifugation at 10,000 x g for 3 min (4 °C), snap frozen in liquid nitrogen and then stored at -  
745 80 °C until processed for RNA extraction. Gene expression in liquid grown cells was analyzed  
746 as follows: cells from overnight YPD cultures were harvested by centrifugation, washed and  
747 resuspended at an OD<sub>600</sub> ≈ 25 in pre-warmed liquid medium and incubated at 37 °C for 2- and  
748 4- h before harvesting the cells by centrifugation; the cell pellets were snap frozen in liquid  
749 nitrogen. For arginine catabolic gene expression analysis, SC5314 was used as wildtype strain.  
750 Briefly, cells from log phase YPD culture growing at 30 °C were harvested, washed 3X with  
751 PBS, diluted in pre-warmed YNB+Arg medium (pH = 6.0, without BCP) at an OD<sub>600</sub> ≈ 0.5, and  
752 then incubated for 1 h at 37 °C under aeration. A portion of the washed cells were snap-frozen  
753 in liquid nitrogen to serve as reference (t = 0). Following 1 h incubation, cells in YNB+Arg were  
754 immediately harvested and then snap-frozen in liquid nitrogen for RNA extraction. To analyze

755 the dependence of *GAP* genes expression to SPS pathway (i.e., *Ssy1*), wildtype (PMRCA18) and  
756 *ssy1Δ/Δ* (YJA64) cells were grown to log phase in SD medium at 30 °C before spiking with 1  
757 mM of glutamine or ddH<sub>2</sub>O for 30 min. Cells were collected from induced (glutamine) and non-  
758 induced (ddH<sub>2</sub>O) cultures and snap-frozen in liquid nitrogen.

759 Total RNA was extracted from frozen cell pellets using RiboPure-Yeast Kit (Ambion®, Life  
760 Technologies) essentially following the instructions of the supplier with the exception that cells  
761 were subjected to extra bead-beating step (Bio-Spec; 1 × 60 sec, 4 M/s). DNase-treated RNA  
762 extracts were reverse-transcribed using SuperScript III and Random Primers (Invitrogen, Life  
763 Technologies). cDNA preparations were diluted 1/40 in ddH<sub>2</sub>O and 5 μl were used as template  
764 for qPCR using KAPA SYBR Green (Kapa Biosystems). Gene specific primers (500 nM) were  
765 added and reactions were performed in a Rotor-Gene 6000 (software version 1.7). The  $\Delta\Delta C_t$   
766 method ( $2^{-\Delta\Delta C_t}$ ) was used to quantitate the relative levels of gene expression.

767

#### 768 **ATP quantification**

769 A bioluminescence-based ATP detection kit (Molecular Probes, Invitrogen) was used to quantify  
770 ATP levels in macrocolonies grown on SXD medium as indicated. ATP was extracted from  
771 eight, 24 h-old macrocolonies harvested using a sterile glass slide and then suspended in 1 ml  
772 sterile ice-cold Tris Buffered Saline (TBS; 50 mM Tris-Cl, pH 7.5, 150 mM NaCl). Cells were  
773 harvested at 10,000 x g for 3 min (4°C) before re-suspending the entire pellet in TCA buffer  
774 containing 100 mM Tris-HCl (pH = 8.0), 10% trichloroacetic acid (TCA), 25 mM ammonium  
775 acetate, and 4 mM EDTA. Cell suspension was transferred to pre-chilled tubes containing glass  
776 beads and then subjected to bead beating (Bio-Spec; 5 × 1 min, 4 M/s with 2 min on ice between  
777 pulses). Cell lysates were collected and a portion of the supernatant was analyzed for ATP  
778 following the instruction of the manufacturer. Luminescence was analyzed using microplate  
779 reader (Berthold) using 1 sec integration time. A portion of the same lysate was used to  
780 determine total protein concentration using the bicinchoninic acid (BCA; Sigma) assay. Results  
781 presented are average of ATP normalized to total protein concentration analyzed from 3  
782 biological replicates; each replicate is an average of 2-3 technical replicates.

783

784 **Immunoblotting**

785 For Stp2 cleavage analysis, cells expressing Stp2-HA (PMRCA48) were grown to saturation in  
786 SD liquid medium overnight at 30 °C and then refreshed the following morning in 25 ml of fresh  
787 SD medium at a starting OD<sub>600</sub> ≈ 0.3. Cells were grown in a 30 °C-shaker to an OD<sub>600</sub> of 1.5-  
788 2.2. For induction experiments, a 500-μl aliquot of log phase culture were separately added to  
789 tubes containing the indicated amount and type of amino acids or an equal volume of water for  
790 control, and then incubated for 5 min at 30 °C in a thermoblock shaking at 700 rpm. For Put2-  
791 HA expression analysis, cells from overnight YPD cultures were harvested, washed and then  
792 grown as indicated. Whole cell lysates were prepared using NaOH/TCA method as described  
793 previously with minor modifications [94]. Cells were lysed on ice with 280 μl of ice-cold 1.85  
794 M NaOH with 7% β-Mercaptoethanol for 15 min; proteins were precipitated ON at 4 °C by  
795 adding the same volume of cold 50% TCA. Protein pellets were quickly washed with ice-cold 1  
796 M Tris base (pH = 11) and then resuspended in equal volume of Tris-HCl (pH = 8.0). In some  
797 instances, as indicated, due to highly variability in protein recovered from certain types of cells  
798 (i.e., yeast and filamentous forms) sample loading was normalized based on protein content.  
799 Samples were denatured in 2X SDS sample buffer at 95-100 °C for 5 min, the proteins were  
800 resolved in sodium dodecyl sulfate-polyacrylamide gel electrophoresis (SDS-PAGE) using 4-  
801 12% pre-cast gels (Invitrogen) and analyzed by immunoblotting on nitrocellulose membrane  
802 according to standard procedure. For Stp2-HA and Put-HA detection, HRP-conjugated anti-HA  
803 antibody (Pierce) was used at 1:2,500 dilution. For loading control, HRP-conjugated rat  
804 monoclonal α-tubulin antibody [YOL1/34] (Abcam) was used at 1:10,000 dilution. Membranes  
805 were blocked using TBST (TBS + 0.1% Tween) containing 10% skimmed milk; antibodies were  
806 diluted in TBST containing 5% skimmed milk. Immunoreactive bands were visualized by  
807 enhanced chemiluminescent detection system (SuperSignal Dura West Extended Duration  
808 Substrate; Pierce) using ChemiDoc MP system (BioRad). Densitometric analyses were  
809 performed using ImageJ.

810

811 **Active Ras1-Pull Down Assay**

812 Active Ras1 (Ras1-GTP) was analyzed in macrocolonies using Pierce Active Ras Pull-Down Kit  
813 (Thermo Scientific) following the manufacturer's instructions, but with an extra bead-beating  
814 step to ensure optimal disruption of cells. Five 24 h-old macrocolonies were scraped, pooled,  
815 and suspended in 1 ml ice-cold TBS in 2-ml microcentrifuge tubes (with caps). Cells were  
816 collected by centrifugation at 10,000 x g for 3 min (4 °C) and then resuspended in 400 µl of  
817 Lysis/Binding/Washing buffer (1X, Pierce kit) supplemented with protease cocktail  
818 (cOmplete™ mini, EDTA-free; Roche) and 1 mM PMSF. Pre-chilled glass beads were added,  
819 cell suspensions were subjected to multiple cycles of bead beating (6 × 40 sec, 4 M/s, 2 min on  
820 ice between pulses). After an initial clarification step at 1,000 rpm for 5 min, supernatants were  
821 collected and total protein was determined using the BCA assay. The concentration of protein in  
822 lysates was adjusted to 2 mg/ml using the lysis buffer as diluent and then 500 µg of protein was  
823 used for the immunoprecipitation. We used 12.5 µg protein for input and eluted bound protein  
824 in 25 µl. Proteins were resolved by SDS-PAGE and analyzed by immunoblotting. Total Ras and  
825 active Ras-GTP were probed with primary monoclonal anti-Ras clone X (1:300) included in the  
826 kit, and secondary goat anti-mouse antibody (1:10,000; Pierce). For loading control, α-tubulin  
827 conjugated to HRP (1:10,000) was used. Membranes were blocked and the primary antibody  
828 diluted in TBST containing 3% BSA; the secondary and loading control antibodies were diluted  
829 in TBST containing 5% skimmed milk. Results presented are representative of at least 3  
830 independent experiments.

831

832 **Growth Assays**

833 For drop plates, cells from log phase YPD cultures grown at 30 °C were harvested, washed, and  
834 then adjusted to OD<sub>600</sub> ≈ 1. Five microliters of 10-fold serially diluted cell suspension were  
835 spotted onto the surface of the indicated SXD media and incubated at 30 °C for 2-3 days and  
836 photographed. For liquid assays, washed cells from log phase YPD cultures were diluted in the  
837 indicated SXD liquid medium to a starting OD<sub>600</sub> ≈ 0.05, and 300 µl were transferred into each  
838 well of a 10 x 10-well microplate and grown continuously for > 20 h at 30 °C with constant

839 agitation. OD<sub>600</sub> readouts were captured using BioScreen C MBR analyzer (Oy Growth Curves  
840 Ab Ltd, Helsinki, Finland).

841

#### 842 **Resazurin Reduction Assay**

843 The membrane permeant, non-destructive redox indicator, Resazurin (Sigma), was used to  
844 measure the metabolic activity of intact cells growing in SXD. Briefly, cells from overnight YPD  
845 cultures were harvested, washed once with sterile ddH<sub>2</sub>O, and adjusted to OD<sub>600</sub> ≈ 0.01 (~3 x  
846 10<sup>5</sup> CFU/ml) using the YNB-glucose base medium (~1.05x strength, pH = 6.0). Using a multi-  
847 channel pipette, 95 µl of this cell suspension were added to the well of a 96-well microplate  
848 followed by addition of 5 µl of 200 mM amino acid stock (10 mM final concentration). Plates  
849 were incubated at 37°C for 2 h with agitation protected from light. After 2 h, 20 µl of filtered  
850 Resazurin dye (0.15 mg/ml) was added to each well and incubated for 2 h at 37 °C before  
851 measuring the fluorescence (560 nm excitation/590 nm emission) using EnSpire microplate  
852 reader (PerkinElmer).

853

#### 854 **TTC Overlay Assay**

855 Macrocolonies grown on the indicated plates for 24 h were overlaid with 2 ml of molten TTC-  
856 agar solution (50-55 °C) containing 0.1% TTC (2,3,5 triphenyltetrazolium chloride; Sigma)  
857 dissolved in 6.7 mM potassium phosphate buffer (PPB, pH = 7.0) with 1% agar [15]. Plates were  
858 photographed 30 min after the overlaid solution became solid.

859

#### 860 **Extracellular oxygen consumption assay**

861 Oxygen consumption assay was performed in *C. albicans* grown in synthetic proline medium  
862 containing the indicated carbon source (i.e., 2% glucose (SPD), 0.2% (SPD<sub>0.2%</sub>), or 1% glycerol  
863 (SPG) using the Extracellular Oxygen Consumption Assay (Abcam, ab197243) following  
864 manufacturer's protocol. Briefly, cells from log phase YPD culture were harvested, washed 3X  
865 with PBS, and then diluted in the indicated media at OD<sub>600</sub> ≈ 0.3. A 150 µl cell suspension was

866 added into each well of a 96-well microplate with black walls and clear bottom. Ten microliters  
867 (10  $\mu$ l) of Extracellular Oxygen Consumption Reagent or medium were then added into each  
868 well, mixed gently by moving the plate on a circular motion, and then spiked with either medium  
869 or control. FCCP (final conc. 10  $\mu$ M) and antimycin (final conc. 10  $\mu$ g/ml) were used as positive  
870 and negative controls, respectively. Plates were analyzed using Enspire microplate reader using  
871 Time Resolved Fluorescence (TRF). Signals were read every 90 sec for 120 repeats with optimal  
872 delay time of 30  $\mu$ s and gate (integration) time of 100  $\mu$ s. Signal from wells without cells were  
873 used as background signal.

874

### 875 **Quantification of proline**

876 The concentration of proline in media and in cell extracts was analyzed using the quantitative  
877 ninhydrin method [95]. Proline utilization was assessed as follows: cells grown overnight in  
878 YPD were washed and resuspended to an  $OD_{600} \approx 0.5$  in pre-warmed synthetic proline media  
879 containing 10 mM of proline and the indicated carbon source. The cultures were incubated under  
880 constant aeration for 2 h at 37 °C, and the amount of proline in culture supernatants was analyzed.  
881 Proline utilization was defined by comparison to non-inoculated media.

882

### 883 ***C. albicans* co-culture with murine macrophages**

884 The murine macrophage cell line RAW264.7 (ATCC) was cultured and passaged in Dulbecco's  
885 modified Eagle's medium/high glucose (HyClone, GE Healthcare Life Sciences, Amersham,  
886 UK) supplemented with 10% fetal bovine serum, 100 U/ml penicillin and 100  $\mu$ g/ml  
887 streptomycin (hereafter referred as D10) at 37°C with 5% CO<sub>2</sub>. Prior to co-culture with *C.*  
888 *albicans*, RAW264.7 cells ( $1 \times 10^6$ ) in D10 medium were seeded on a 24-well microplate  
889 containing sterile cover slips and were allowed to adhere overnight in a humidified chamber at  
890 37°C and 5% CO<sub>2</sub>. Fungal cells ( $3 \times 10^8$ ) were harvested from overnight YPD cultures and  
891 stained with 1 mg/ml FITC solution in 0.1 M NaHCO<sub>3</sub> buffer (pH = 9.0) in the dark for 15 min  
892 at 30 °C. Cells were washed 3X with PBS before resuspending in equal volume of PBS. Fungal  
893 cells were added to macrophage at MOI of 3:1 (*Candida*:Macrophage, C:M) and were then

894 allowed to interact for 30 min. Non-phagocytosed cells were removed by washing the cells at  
895 least 5X with pre-warmed Hank's Balanced Salt Solution (HBSS) and 1X with D10 medium.  
896 Cells were allowed to interact for an additional 4 h in fresh D10 medium before fixing with 3.7%  
897 formaldehyde-PBS for 15 min in the dark at room temperature. Fixed cells were then washed  
898 3X with PBS before staining with calcofluor white (10 µg/ml) for 1 min. After 2X PBS washing,  
899 coverslips were mounted on glass slides using ProLong™ Gold antifade reagent (Invitrogen).  
900 Images were obtained using LSM 800, 63x/1.2 oil.

901

### 902 ***C. albicans* killing by murine macrophages**

903 The survival of *C. albicans* co-cultured with macrophages was assessed by colony forming units  
904 (CFU) analysis. Briefly, RAW264.7 cells in D10 were seeded into a 96-well microplate at a  
905 density of  $1 \times 10^5$  per 200 µl and allowed to adhere overnight. *C. albicans* cells from overnight  
906 YPD cultures were processed without staining and added at a MOI of 3:1 (C:M). The co-cultures  
907 were incubated for 3 h prior to assessing fungal cell viability by CFU; each well was treated to  
908 final concentration of 0.1 % Triton X-100 for 2 min to lyse macrophage and serial dilutions were  
909 prepared and plated onto YPD. CFUs were counted 2 days after incubation at 30 °C. The ability  
910 of macrophages to kill *C. albicans* (% killing) was determined by comparison of fungal CFU  
911 recovered in the absence of macrophages.

912

### 913 **Indirect immunofluorescence microscopy of phagocytosed *C. albicans***

914 RAW264.7 cells were co-cultured with *C. albicans* cells, CFG185 (*PUT2/PUT2-HA*), for 90 min  
915 on glass coverslips at a MOI of 5:1 (C:M). Cells were fixed in 3.7% formaldehyde-PBS for 15  
916 min, and permeabilized in 0.25% Tween-20 for 15 min, both incubations were at room  
917 temperature. The fixed and permeabilized cells were incubated in zymolyase buffer (2U  
918 zymolyase 100T (Zymo Research, Irvine, CA, USA), 10 mM DTT in PBS) for 1 h at 30 °C.  
919 After washing, cells were incubated at room temperature in 0.25% Tween-20 for 10 min and  
920 blocked in 5% FBS for 30 min. Cells were incubated overnight at 4 °C with rat anti-HA (Roche,  
921 Germany, #1867423) and rabbit anti-Lamp1 (Abcam, UK, #ab24170) primary antibodies diluted

922 1:500 in 0.25% Tween-20. Cells were washed with PBS and incubated 2 h with Alexa flour 488  
923 goat anti-rabbit (Invitrogen, Eugene, OR, USA #A11034) and Alexa flour 555 goat anti-rat  
924 (Invitrogen, Eugene, OR, USA #A11034) secondary antibodies diluted 1:500 in 0.25% Tween-  
925 20. Images were captured on a Zeiss 510 Meta confocal microscope, 63x/1.4 oil. Orthogonal  
926 views were constructed in FIJI imaging software.

927

928

## 929 **Acknowledgments**

930 The authors would like to thank the members of Claes Andréasson, Martin Ott, and Per  
931 Ljungdahl laboratories (SU), and members of the Marie Curie-ITN ImResFun program for  
932 constructive comments throughout the course of this work. Gratitude is extended to Valmik Vyas  
933 and Gerard Fink (MIT, Cambridge, MA, USA) for providing the CRISPR/Cas9 cassettes and for  
934 the valuable suggestions. Patrick van Dijck (KUL, Leuvan, Belgium), Karl Kuchler (MUV,  
935 Vienna, Austria), Kenneth Nickerson and Ruvini Pathirana (UNL, Lincoln, NE, USA) are  
936 gratefully acknowledged for supplying strains and discussions; and Nora Grahl and Deborah  
937 Hogan (Dartmouth Medical School, Hanover, NH, USA) for helpful discussions. We also thank  
938 Stina Höglund, the Imaging Facility-Stockholm University, for assistance in microscopy. This  
939 work was supported by EU grant MC-ITN-606786 (ImResFun) and Swedish Research Council  
940 VR-2015-04202 (POL).

941

942

## 943 **References**

- 944 1. Moyes DL, Naglik JR. Mucosal immunity and *Candida albicans* infection. Clin Dev  
945 Immunol. 2011;2011:346307. doi: 10.1155/2011/346307.
- 946 2. Kullberg BJ, Arendrup MC. Invasive Candidiasis. N Engl J Med. 2015;373(15):1445-56.  
947 doi: 10.1056/NEJMra1315399.

- 948 3. Brown AJ, Brown GD, Netea MG, Gow NA. Metabolism impacts upon *Candida*  
949 immunogenicity and pathogenicity at multiple levels. *Trends Microbiol.* 2014;22(11):614-  
950 22. doi: 10.1016/j.tim.2014.07.001.
- 951 4. Sudbery PE. Growth of *Candida albicans* hyphae. *Nat Rev Microbiol.* 2011;9(10):737-48.  
952 doi: 10.1038/nrmicro2636.
- 953 5. Berman J. Morphogenesis and cell cycle progression in *Candida albicans*. *Curr Opin*  
954 *Microbiol.* 2006;9(6):595-601. doi: 10.1016/j.mib.2006.10.007.
- 955 6. Sudbery P, Gow N, Berman J. The distinct morphogenic states of *Candida albicans*. *Trends*  
956 *Microbiol.* 2004;12(7):317-24. doi: 10.1016/j.tim.2004.05.008.
- 957 7. Noble SM, Gianetti BA, Witchley JN. *Candida albicans* cell-type switching and functional  
958 plasticity in the mammalian host. *Nat Rev Microbiol.* 2016. doi: 10.1038/nrmicro.2016.157.
- 959 8. Lo HJ, Kohler JR, DiDomenico B, Loebenberg D, Cacciapuoti A, Fink GR. Nonfilamentous  
960 *C. albicans* mutants are avirulent. *Cell.* 1997;90(5):939-49.
- 961 9. Lorenz MC, Bender JA, Fink GR. Transcriptional response of *Candida albicans* upon  
962 internalization by macrophages. *Eukaryot Cell.* 2004;3(5):1076-87. doi:  
963 10.1128/EC.3.5.1076-1087.2004.
- 964 10. Braun BR, D. JA. *TUP1*, *CPH1* and *EFG1* make independent contributions to filamentation  
965 in *Candida albicans*. *Genetics.* 2000;155:56-67.
- 966 11. Land GA, McDonald WC, Stjernholm RL, Friedman L. Factors affecting filamentation in  
967 *Candida albicans*: changes in respiratory activity of *Candida albicans* during filamentation.  
968 *Infect Immun.* 1975;12(1):119-27.
- 969 12. Land GA, McDonald WC, Stjernholm RL, Friedman TL. Factors affecting filamentation in  
970 *Candida albicans*: relationship of the uptake and distribution of proline to morphogenesis.  
971 *Infect Immun.* 1975;11(5):1014-23.
- 972 13. Dabrowa N, Taxer SS, Howard DH. Germination of *Candida albicans* induced by proline.  
973 *Infect Immun.* 1976;13(3):830-5.
- 974 14. Grahl N, Demers EG, Lindsay AK, Harty CE, Willger SD, Piispanen AE, et al.  
975 Mitochondrial Activity and *Cyr1* Are Key Regulators of *Ras1* Activation of *C. albicans*

- 976 Virulence Pathways. PLoS Pathog. 2015;11(8):e1005133. doi:  
977 10.1371/journal.ppat.1005133.
- 978 15. Morales DK, Grahl N, Okegbe C, Dietrich LE, Jacobs NJ, Hogan DA. Control of *Candida*  
979 *albicans* metabolism and biofilm formation by *Pseudomonas aeruginosa* phenazines. MBio.  
980 2013;4(1):e00526-12. doi: 10.1128/mBio.00526-12.
- 981 16. Watanabe T, Ogasawara A, Mikami T, Matsumoto T. Hyphal formation of *Candida*  
982 *albicans* is controlled by electron transfer system. Biochem Biophys Res Commun.  
983 2006;348(1):206-11. doi: 10.1016/j.bbrc.2006.07.066.
- 984 17. Monge RA, Roman E, Nombela C, Pla J. The MAP kinase signal transduction network in  
985 *Candida albicans*. Microbiology. 2006;152(Pt 4):905-12. doi: 10.1099/mic.0.28616-0.
- 986 18. Stoldt VR, Sonneborn A, Leuker CE, Ernst JF. Efg1p, an essential regulator of  
987 morphogenesis of the human pathogen *Candida albicans*, is a member of a conserved class  
988 of bHLH proteins regulating morphogenetic processes in fungi. EMBO J. 1997;16(8):1982-  
989 91. doi: 10.1093/emboj/16.8.1982.
- 990 19. Biswas S, Van Dijck P, Datta A. Environmental sensing and signal transduction pathways  
991 regulating morphopathogenic determinants of *Candida albicans*. Microbiol Mol Biol Rev.  
992 2007;71(2):348-76. doi: 10.1128/MMBR.00009-06.
- 993 20. Hogan DA, Sundstrom P. The Ras/cAMP/PKA signaling pathway and virulence in *Candida*  
994 *albicans*. Future Microbiol. 2009;4(10):1263-70. doi: 10.2217/fmb.09.106.
- 995 21. Leberer E, Harcus D, Dignard D, Johnson L, Ushinsky S, Thomas DY, et al. Ras links  
996 cellular morphogenesis to virulence by regulation of the MAP kinase and cAMP signalling  
997 pathways in the pathogenic fungus *Candida albicans*. Mol Microbiol. 2001;42(3):673-87.
- 998 22. Feng Q, Summers E, Guo B, Fink G. Ras signaling is required for serum-induced hyphal  
999 differentiation in *Candida albicans*. J Bacteriol. 1999;181(20):6339-46.
- 1000 23. Inglis DO, Sherlock G. Ras signaling gets fine-tuned: regulation of multiple pathogenic  
1001 traits of *Candida albicans*. Eukaryot Cell. 2013;12(10):1316-25. doi: 10.1128/EC.00094-  
1002 13.

- 1003 24. Fang HM, Wang Y. RA domain-mediated interaction of Cdc35 with Ras1 is essential for  
1004 increasing cellular cAMP level for *Candida albicans* hyphal development. *Mol Microbiol.*  
1005 2006;61(2):484-96. doi: 10.1111/j.1365-2958.2006.05248.x.
- 1006 25. Zou H, Fang HM, Zhu Y, Wang Y. *Candida albicans* Cyr1, Cap1 and G-actin form a  
1007 sensor/effector apparatus for activating cAMP synthesis in hyphal growth. *Mol Microbiol.*  
1008 2010;75(3):579-91. doi: 10.1111/j.1365-2958.2009.06980.x.
- 1009 26. Rocha CR, Schroppel K, Harcus D, Marciel A, Dignard D, Taylor BN, et al. Signaling  
1010 through adenylyl cyclase is essential for hyphal growth and virulence in the pathogenic  
1011 fungus *Candida albicans*. *Mol Biol Cell.* 2001;12(11):3631-43.
- 1012 27. Hogan DA, Muhlschlegel FA. *Candida albicans* developmental regulation: adenylyl cyclase  
1013 as a coincidence detector of parallel signals. *Curr Opin Microbiol.* 2011;14(6):682-6. doi:  
1014 10.1016/j.mib.2011.09.014.
- 1015 28. Wang Y. Fungal adenylyl cyclase acts as a signal sensor and integrator and plays a central  
1016 role in interaction with bacteria. *PLoS Pathog.* 2013;9(10):e1003612. doi:  
1017 10.1371/journal.ppat.1003612.
- 1018 29. Klengel T, Liang WJ, Chaloupka J, Ruoff C, Schroppel K, Naglik JR, et al. Fungal adenylyl  
1019 cyclase integrates CO<sub>2</sub> sensing with cAMP signaling and virulence. *Curr Biol.*  
1020 2005;15(22):2021-6. doi: 10.1016/j.cub.2005.10.040.
- 1021 30. Ghosh S, Navarathna DH, Roberts DD, Cooper JT, Atkin AL, Petro TM, et al. Arginine-  
1022 induced germ tube formation in *Candida albicans* is essential for escape from murine  
1023 macrophage line RAW 264.7. *Infect Immun.* 2009;77(4):1596-605. doi:  
1024 10.1128/IAI.01452-08.
- 1025 31. Maidan MM, Thevelein JM, Van Dijck P. Carbon source induced yeast-to-hypha transition  
1026 in *Candida albicans* is dependent on the presence of amino acids and on the G-protein-  
1027 coupled receptor Gpr1. *Biochem Soc Trans.* 2005;33(Pt 1):291-3. doi:  
1028 10.1042/BST0330291.
- 1029 32. Miwa T, Takagi Y, Shinozaki M, Yun CW, Schell WA, Perfect JR, et al. Gpr1, a putative  
1030 G-protein-coupled receptor, regulates morphogenesis and hypha formation in the

- 1031 pathogenic fungus *Candida albicans*. Eukaryot Cell. 2004;3(4):919-31. doi:  
1032 10.1128/EC.3.4.919-931.2004.
- 1033 33. Ballou ER, Avelar GM, Childers DS, Mackie J, Bain JM, Wagener J, et al. Lactate signalling  
1034 regulates fungal beta-glucan masking and immune evasion. Nat Microbiol. 2016;2:16238.  
1035 doi: 10.1038/nmicrobiol.2016.238.
- 1036 34. Martínez P, Ljungdahl PO. Divergence of Stp1 and Stp2 transcription factors in *Candida*  
1037 *albicans* places virulence factors required for proper nutrient acquisition under amino acid  
1038 control. Mol Cell Biol. 2005;25(21):9435-46. doi: 10.1128/MCB.25.21.9435-9446.2005.
- 1039 35. Martínez P, Ljungdahl PO. An ER packaging chaperone determines the amino acid uptake  
1040 capacity and virulence of *Candida albicans*. Mol Microbiol. 2004;51(2):371-84. doi:  
1041 10.1046/j.1365-2958.2003.03845.x.
- 1042 36. Brega E, Zufferey R, Mamoun CB. *Candida albicans* Csy1p is a nutrient sensor important  
1043 for activation of amino acid uptake and hyphal morphogenesis. Eukaryot Cell.  
1044 2004;3(1):135-43.
- 1045 37. Dabas N, Morschhäuser J. A transcription factor regulatory cascade controls secreted  
1046 aspartic protease expression in *Candida albicans*. Mol Microbiol. 2008;69(3):586-602. doi:  
1047 10.1111/j.1365-2958.2008.06297.x.
- 1048 38. Felk A, Kretschmar M, Albrecht A, Schaller M, Beinhauer S, Nichterlein T, et al. *Candida*  
1049 *albicans* hyphal formation and the expression of the Efg1-regulated proteinases Sap4 to  
1050 Sap6 are required for the invasion of parenchymal organs. Infect Immun. 2002;70(7):3689-  
1051 700.
- 1052 39. Hall MP, Unch J, Binkowski BF, Valley MP, Butler BL, Wood MG, et al. Engineered  
1053 luciferase reporter from a deep sea shrimp utilizing a novel imidazopyrazinone substrate.  
1054 ACS Chem Biol. 2012;7(11):1848-57. doi: 10.1021/cb3002478.
- 1055 40. Liu H, Kohler J, Fink GR. Suppression of hyphal formation in *Candida albicans* by mutation  
1056 of a *STE12* homolog. Science. 1994;266(5191):1723-6.
- 1057 41. Custot J, Moali C, Brollo M, Boucher JL, Delaforge M, Mansuy D, et al. A new  $\alpha$ -amino  
1058 acid N-w-hydroxy-nor-L-arginine: A highly-affinity inhibitor of arginase well adapted to

- 1059 bind to its manganese cluster. *J Am Chem Soc.* 1997;119(17):4086-7. doi:  
1060 10.1021/ja970285o.
- 1061 42. Zhang M, White TA, Schuermann JP, Baban BA, Becker DF, Tanner JJ. Structures of the  
1062 *Escherichia coli* PutA proline dehydrogenase domain in complex with competitive  
1063 inhibitors. *Biochemistry.* 2004;43(39):12539-48. Epub 2004/09/29. doi:  
1064 10.1021/bi048737e.
- 1065 43. Zhu W, Gincherman Y, Docherty P, Spilling CD, Becker DF. Effects of proline analog  
1066 binding on the spectroscopic and redox properties of PutA. *Arch Biochem Biophys.*  
1067 2002;408(1):131-6.
- 1068 44. Rich PR, Mischis LA, Purton S, Wiskich JT. The sites of interaction of triphenyltetrazolium  
1069 chloride with mitochondrial respiratory chains. *FEMS Microbiol Lett.* 2001;202(2):181-7.
- 1070 45. Candeias LP, MacFarlane DPS, S.L.W. M, Maidwell NL, Roeschlaub CA, Sammes PG, et  
1071 al. The catalysed NADH reduction of resazurin to resorufin. *J Chem Soc.* 1998;(11):2333–  
1072 4. doi: 10.1039/A806431H.
- 1073 46. Tebung WA, Omran RP, Fulton DL, Morschhäuser J, Whiteway M. Put3 positively  
1074 regulates proline utilization in *Candida albicans*. *mSphere.* 2017;2(6). Epub 2017/12/16.  
1075 doi: 10.1128/mSphere.00354-17.
- 1076 47. Vylkova S, Carman AJ, Danhof HA, Collette JR, Zhou H, Lorenz MC. The fungal pathogen  
1077 *Candida albicans* autoinduces hyphal morphogenesis by raising extracellular pH. *MBio.*  
1078 2011;2(3):e00055-11. doi: 10.1128/mBio.00055-11.
- 1079 48. Vemuri GN, Eiteman MA, McEwen JE, Olsson L, Nielsen J. Increasing NADH oxidation  
1080 reduces overflow metabolism in *Saccharomyces cerevisiae*. *Proc Natl Acad Sci U S A.*  
1081 2007;104(7):2402-7. doi: 10.1073/pnas.0607469104.
- 1082 49. Kayikci O, Nielsen J. Glucose repression in *Saccharomyces cerevisiae*. *FEMS Yeast Res.*  
1083 2015;15(6). Epub 2015/07/25. doi: 10.1093/femsyr/fov068.
- 1084 50. Ljungdahl PO, Daignan-Fornier B. Regulation of amino acid, nucleotide, and phosphate  
1085 metabolism in *Saccharomyces cerevisiae*. *Genetics.* 2012;190(3):885-929. doi:  
1086 10.1534/genetics.111.133306.

- 1087 51. Liao WL, Ramon AM, Fonzi WA. *GLN3* encodes a global regulator of nitrogen metabolism  
1088 and virulence of *C. albicans*. *Fungal Genet Biol.* 2008;45(4):514-26. doi:  
1089 10.1016/j.fgb.2007.08.006.
- 1090 52. Skrzypek MS, Binkley J, Binkley G, Miyasato SR, Simison M, Sherlock G. The *Candida*  
1091 Genome Database (CGD): incorporation of Assembly 22, systematic identifiers and  
1092 visualization of high throughput sequencing data. *Nucleic Acids Res.* 2017;45(D1):D592-  
1093 D6. Epub 2016/10/16. doi: 10.1093/nar/gkw924.
- 1094 53. Holmes AR, Shepherd MG. Proline-induced germ-tube formation in *Candida albicans*: role  
1095 of proline uptake and nitrogen metabolism. *J Gen Microbiol.* 1987;133(11):3219-28.
- 1096 54. Brandriss MC, Magasanik B. Genetics and physiology of proline utilization in  
1097 *Saccharomyces cerevisiae*: enzyme induction by proline. *J Bacteriol.* 1979;140(2):498-503.
- 1098 55. Brandriss MC, Magasanik B. Proline: an essential intermediate in arginine degradation in  
1099 *Saccharomyces cerevisiae*. *J Bacteriol.* 1980;143(3):1403-10.
- 1100 56. Brandriss MC, Magasanik B. Subcellular compartmentation in control of converging  
1101 pathways for proline and arginine metabolism in *Saccharomyces cerevisiae*. *J Bacteriol.*  
1102 1981;145(3):1359-64.
- 1103 57. Steegborn C. Structure, mechanism, and regulation of soluble adenylyl cyclases -  
1104 similarities and differences to transmembrane adenylyl cyclases. *Biochim Biophys Acta.*  
1105 2014;1842(12 Pt B):2535-47. Epub 2014/09/07. doi: 10.1016/j.bbadis.2014.08.012.
- 1106 58. Xue Y, Batlle M, Hirsch JP. *GPR1* encodes a putative G protein-coupled receptor that  
1107 associates with the Gpa2p Galpha subunit and functions in a Ras-independent pathway.  
1108 *EMBO J.* 1998;17(7):1996-2007. doi: 10.1093/emboj/17.7.1996.
- 1109 59. Maidan MM, De Rop L, Serneels J, Exler S, Rupp S, Tournu H, et al. The G protein-coupled  
1110 receptor Gpr1 and the Galpha protein Gpa2 act through the cAMP-protein kinase A pathway  
1111 to induce morphogenesis in *Candida albicans*. *Mol Biol Cell.* 2005;16(4):1971-86. doi:  
1112 10.1091/mbc.E04-09-0780.
- 1113 60. Bicho CC, de Lima Alves F, Chen ZA, Rappsilber J, Sawin KE. A genetic engineering  
1114 solution to the "arginine conversion problem" in stable isotope labeling by amino acids in

- 1115 cell culture (SILAC). *Mol Cell Proteomics*. 2010;9(7):1567-77. doi:  
1116 10.1074/mcp.M110.000208.
- 1117 61. Park SK, Liao L, Kim JY, Yates JR, 3rd. A computational approach to correct arginine-to-  
1118 proline conversion in quantitative proteomics. *Nat Methods*. 2009;6(3):184-5. Epub  
1119 2009/02/28. doi: 10.1038/nmeth0309-184.
- 1120 62. Lossner C, Warnken U, Pscherer A, Schnolzer M. Preventing arginine-to-proline conversion  
1121 in a cell-line-independent manner during cell cultivation under stable isotope labeling by  
1122 amino acids in cell culture (SILAC) conditions. *Anal Biochem*. 2011;412(1):123-5. Epub  
1123 2011/01/19. doi: 10.1016/j.ab.2011.01.011.
- 1124 63. Van Hoof D, Pinkse MW, Oostwaard DW, Mummery CL, Heck AJ, Krijgsveld J. An  
1125 experimental correction for arginine-to-proline conversion artifacts in SILAC-based  
1126 quantitative proteomics. *Nat Methods*. 2007;4(9):677-8. Epub 2007/09/01. doi:  
1127 10.1038/nmeth0907-677.
- 1128 64. Nickerson WJ, and Edwards, G.A. Studies on the physiological bases of morphogenesis in  
1129 fungi. I. The respiratory metabolism of dimorphic pathogenic fungi. *J Gen Physiol*.  
1130 1949;33(1):41-55.
- 1131 65. Gancedo JM. Yeast carbon catabolite repression. *Microbiol Mol Biol Rev*. 1998;62(2):334-  
1132 61. Epub 1998/06/10.
- 1133 66. Pronk JT, Yde Steensma H, Van Dijken JP. Pyruvate metabolism in *Saccharomyces*  
1134 *cerevisiae*. *Yeast*. 1996;12(16):1607-33. Epub 1996/12/01. doi: 10.1002/(SICI)1097-  
1135 0061(199612)12:16<1607::AID-YEA70>3.0.CO;2-4.
- 1136 67. Niimi M, Kamiyama A, Tokunaga M. Respiration of medically important *Candida* species  
1137 and *Saccharomyces cerevisiae* in relation to glucose effect. *J Med Vet Mycol*.  
1138 1988;26(3):195-8. Epub 1988/06/01.
- 1139 68. Sabina J, Brown V. Glucose sensing network in *Candida albicans*: a sweet spot for fungal  
1140 morphogenesis. *Eukaryot Cell*. 2009;8(9):1314-20. doi: 10.1128/EC.00138-09.
- 1141 69. Askew C, Sellam A, Epp E, Hogues H, Mullick A, Nantel A, et al. Transcriptional regulation  
1142 of carbohydrate metabolism in the human pathogen *Candida albicans*. *PLoS Pathog*.  
1143 2009;5(10):e1000612. Epub 2009/10/10. doi: 10.1371/journal.ppat.1000612.

- 1144 70. Johnston M. Feasting, fasting and fermenting. Glucose sensing in yeast and other cells.  
1145 Trends Genet. 1999;15(1):29-33. Epub 1999/03/24.
- 1146 71. Kraidlova L, Schrevens S, Tournu H, Van Zeebroeck G, Sychrova H, Van Dijck P.  
1147 Characterization of the *Candida albicans* amino acid permease family: Gap2 is the only  
1148 general amino acid permease and Gap4 is an S-adenosylmethionine (SAM) transporter  
1149 required for SAM-induced morphogenesis. mSphere. 2016;1(6). Epub 2016/12/29. doi:  
1150 10.1128/mSphere.00284-16.
- 1151 72. Dabrowa N, Howard DH. Proline uptake in *Candida albicans*. J Gen Microbiol.  
1152 1981;127(2):391-7. doi: 10.1099/00221287-127-2-391.
- 1153 73. Jimenez-Lopez C, Collette JR, Brothers KM, Shepardson KM, Cramer RA, Wheeler RT, et  
1154 al. *Candida albicans* induces arginine biosynthetic genes in response to host-derived  
1155 reactive oxygen species. Eukaryot Cell. 2013;12(1):91-100. doi: 10.1128/EC.00290-12.
- 1156 74. Kitamoto K, Yoshizawa K, Ohsumi Y, Anraku Y. Dynamic aspects of vacuolar and  
1157 cytosolic amino acid pools of *Saccharomyces cerevisiae*. J Bacteriol. 1988;170(6):2683-6.
- 1158 75. Martins RM, Covarrubias C, Rojas RG, Silber AM, Yoshida N. Use of L-proline and ATP  
1159 production by *Trypanosoma cruzi* metacyclic forms as requirements for host cell invasion.  
1160 Infect Immun. 2009;77(7):3023-32. Epub 2009/05/13. doi: 10.1128/IAI.00138-09.
- 1161 76. Mantilla BS, Marchese L, Casas-Sanchez A, Dyer NA, Ejeh N, Biran M, et al. Proline  
1162 metabolism is essential for *Trypanosoma brucei brucei* survival in the Tsetse vector. PLoS  
1163 Pathog. 2017;13(1):e1006158. Epub 2017/01/24. doi: 10.1371/journal.ppat.1006158.
- 1164 77. Tonelli RR, Silber AM, Almeida-de-Faria M, Hirata IY, Colli W, Alves MJ. L-proline is  
1165 essential for the intracellular differentiation of *Trypanosoma cruzi*. Cell Microbiol.  
1166 2004;6(8):733-41. Epub 2004/07/09. doi: 10.1111/j.1462-5822.2004.00397.x.
- 1167 78. Ebikeme CE, Peacock L, Coustou V, Riviere L, Bringaud F, Gibson WC, et al. N-acetyl D-  
1168 glucosamine stimulates growth in procyclic forms of *Trypanosoma brucei* by inducing a  
1169 metabolic shift. Parasitology. 2008;135(5):585-94. doi: 10.1017/S0031182008004241.
- 1170 79. Vylkova S, Lorenz MC. Modulation of phagosomal pH by *Candida albicans* promotes  
1171 hyphal morphogenesis and requires Stp2p, a regulator of amino acid transport. PLoS Pathog.  
1172 2014;10(3):e1003995. doi: 10.1371/journal.ppat.1003995.

- 1173 80. Velasco I, Tenreiro S, Calderon IL, André B. *Saccharomyces cerevisiae* Aqr1 is an internal-  
1174 membrane transporter involved in excretion of amino acids. *Eukaryotic Cell*.  
1175 2004;3(6):1492-503. doi: 10.1128/ec.3.6.1492-1503.2004.
- 1176 81. Hess DC, Lu W, Rabinowitz JD, Botstein D. Ammonium toxicity and potassium limitation  
1177 in yeast. *PLoS Biol*. 2006;4(11):e351. Epub 2006/10/20. doi:  
1178 10.1371/journal.pbio.0040351.
- 1179 82. Fleck CB, Schöbel F, Brock M. Nutrient acquisition by pathogenic fungi: Nutrient  
1180 availability, pathway regulation, and differences in substrate utilization. *International*  
1181 *Journal of Medical Microbiology*. 2011;301(5):400-7. doi: 10.1016/j.ijmm.2011.04.007.
- 1182 83. Olive AJ, Sasseti CM. Metabolic crosstalk between host and pathogen: sensing, adapting  
1183 and competing. *Nat Rev Microbiol*. 2016;14(4):221-34. doi: 10.1038/nrmicro.2016.12.
- 1184 84. Yuan X, Mitchell BM, Wilhelmus KR. Expression of matrix metalloproteinases during  
1185 experimental *Candida albicans* keratitis. *Invest Ophthalmol Vis Sci*. 2009;50(2):737-42.  
1186 doi: 10.1167/iovs.08-2390.
- 1187 85. Vyas VK, Barrasa MI, Fink GR. A *Candida albicans* CRISPR system permits genetic  
1188 engineering of essential genes and gene families. *Sci Adv*. 2015;1(3):1-6. doi:  
1189 <http://dx.doi.org/10.1126/sciadv.1500248>.
- 1190 86. Vyas VK, Bushkin GG, Bernstein DA, Getz MA, Sewastianik M, Barrasa MI, et al. New  
1191 CRISPR mutagenesis strategies reveal variation in repair mechanisms among fungi.  
1192 *mSphere*. 2018;3(2). Epub 2018/04/27. doi: 10.1128/mSphere.00154-18.
- 1193 87. Farboud B, J. MB. Dramatic enhancement of genome editing by CRISPR:Cas9 through  
1194 improved guide RNA design. *Genetics*. 2015;199:959-71.
- 1195 88. Reuss O, Vik A, Kolter R, Morschhäuser J. The *SAT1* flipper, an optimized tool for gene  
1196 disruption in *Candida albicans*. *Gene*. 2004;341:119-27. doi: 10.1016/j.gene.2004.06.021.
- 1197 89. Nurk S, Bankevich A, Antipov D, Gurevich AA, Korobeynikov A, Lapidus A, et al.  
1198 Assembling single-cell genomes and mini-metagenomes from chimeric MDA products. *J*  
1199 *Comput Biol*. 2013;20(10):714-37. Epub 2013/10/08. doi: 10.1089/cmb.2013.0084.

- 1200 90. Kolmogorov M, Raney B, Paten B, Pham S. Ragout-a reference-assisted assembly tool for  
1201 bacterial genomes. *Bioinformatics*. 2014;30(12):i302-9. Epub 2014/06/17. doi:  
1202 10.1093/bioinformatics/btu280.
- 1203 91. Minkin I, Pham H, Starostina E, Vyahhi N, Pham S. C-Sibelia: an easy-to-use and highly  
1204 accurate tool for bacterial genome comparison. *F1000Res*. 2013;2:258. Epub 2013/01/01.  
1205 doi: 10.12688/f1000research.2-258.v1.
- 1206 92. Gurevich A, Saveliev V, Vyahhi N, Tesler G. QUASt: quality assessment tool for genome  
1207 assemblies. *Bioinformatics*. 2013;29(8):1072-5. Epub 2013/02/21. doi:  
1208 10.1093/bioinformatics/btt086.
- 1209 93. Masser AE, Kandasamy G, Kaimal JM, Andréasson C. Luciferase NanoLuc as a reporter  
1210 for gene expression and protein levels in *Saccharomyces cerevisiae*. *Yeast*. 2016;33(5):191-  
1211 200. Epub 2016/02/11. doi: 10.1002/yea.3155.
- 1212 94. Silve S, Volland C, Garnier C, Jund R, Chevallier MR, Haguenaer-Tsapis R. Membrane  
1213 insertion of uracil permease, a polytopic yeast plasma membrane protein. *Mol Cell Biol*.  
1214 1991;11(2):1114-24.
- 1215 95. Carillo P, Mastrolonardo G, Nacca F, Parisi D, Verlotta A, Fuggi A. Nitrogen metabolism  
1216 in durum wheat under salinity: accumulation of proline and glycine betaine. *Functional Plant*  
1217 *Biology* [Internet]. 2008; 35(5):[412-26 pp.]. Available from:  
1218 <http://dx.doi.org/10.1071/FP08108>.
- 1219 96. Hnisz D, Majer O, Frohner IE, Komnenovic V, Kuchler K. The Set3/Hos2 histone  
1220 deacetylase complex attenuates cAMP/PKA signaling to regulate morphogenesis and  
1221 virulence of *Candida albicans*. *PLoS Pathog*. 2010;6(5):e1000889. Epub 2010/05/21. doi:  
1222 10.1371/journal.ppat.1000889.
- 1223

1224 **Supporting Information**

1225 **Fig S1. Hyphae-specific gene (*HSG*) expression in *C. albicans* grown in the presence of inducing**  
1226 **amino acids.**

1227 **Fig S2. NanoLuc™ luciferase assay for analysis of Stp2 target gene expression.**

1228 **Fig S3. CRISPR/Cas9-mediated gene inactivation in *C. albicans*.**

1229 **Fig S4. Metabolic activity of *C. albicans* grown in the presence of inducing and non-inducing**  
1230 **amino acids.**

1231 **Fig S5. Growth curves of arginase-pathway mutants in different nitrogen sources.**

1232 **Fig S6. Neutralization of medium containing amino acid as sole carbon and nitrogen source**  
1233 **remains intact in mutant lacking *DUR1,2*.**

1234 **Fig S7. Carbon source and mitochondria-dependent oxygen consumption of *C. albicans*.**

1235 **Table S1. Strains used in this study.**

1236 **Table S2. Primers used in this study**

1237

1238

1239 **Figures**

1240 **Fig 1. Amino acid-induced morphogenesis is dependent on amino acid uptake. A.**

1241 Macrocolonies of wildtype *C. albicans* (PMRCA18) grown on SXD medium containing 10 mM  
1242 of the indicated amino acids (X = Pro, Arg, Orn or Asp) and 2% glucose after 48 h of growth at  
1243 37 °C (upper panels). Cells scraped from macrocolonies stained with calcofluor white (lower  
1244 panels); scale bars = 30 μ. **B.** Amino acid-induced SPS-sensor signaling. Cells expressing Stp2-  
1245 6XHA (PMRCA48) were grown to log phase in SD medium and induced with 50 μM or 5 mM  
1246 of the indicated amino acids for 5 min at 30 °C. The levels of latent and processed Stp2 in extracts  
1247 were analyzed by immunoblotting (upper panels). Similarly, reporter strain (CFG001) carrying  
1248 an integrated P<sub>CANI</sub>-NanoLuc™-PEST construct was grown to log phase in SD medium and  
1249 induced with 50 μM of the indicated amino acids for 2 h at 30 °C. The average luciferase signal

1250 (ave.  $\pm$  CI, 95% CL) are plotted; threshold for significance  $\geq 1.5X$  fold change). **C.**  
1251 Macrocolonies of wildtype (WT; PMRCA18) and strains carrying mutations inactivating SPS-  
1252 sensing pathway components *ssyl* $\Delta/\Delta$  (YJA64), *ssy5* $\Delta/\Delta$  (YJA53), *stp1* $\Delta/\Delta$  (PMRCA59),  
1253 *stp2* $\Delta/\Delta$  (PMRCA57), *stp1* $\Delta/\Delta$  *stp2* $\Delta/\Delta$  (PMRCA94) and *csh3* $\Delta/\Delta$  (PMRCA12) grown on the  
1254 indicated SXD media. **D.** Constitutively active Stp2\* but not Stp1\* bypasses the filamentous  
1255 growth defect of a *ssyl* null mutant in the presence of ornithine. Macrocolonies of WT  
1256 (PMRCA18), *STP1\** (PMRCA23), *STP2\** (PMRCA44), *ssyl*<sup>-/-</sup> *STP1\** (CFG078), and *ssyl*<sup>-/-</sup>  
1257 *STP2\** (CFG073) grown on SQD with ornithine (O) as sole nitrogen source. Images in C and D  
1258 were obtained after 24 h of incubation 37 °C.

1259  
1260 **Fig 2. Amino acid-induced morphogenesis is dependent on catabolism and Ras1 activated**  
1261 **Efg1-dependent transcription.** **A.** Scheme of possible signaling pathways controlling amino  
1262 acid-induced morphogenesis. **B.** Amino acid-induced morphogenesis requires a functional  
1263 Ras1/cAMP/PKA pathway (Efg1-dependent) but not on the MAPK signaling pathway (Cph1-  
1264 dependent). Wildtype (WT; PMRCA18) and strains lacking Ras1 (CDH107), Cph1 (JKC19),  
1265 Efg1 (HLC52), and both Cph1 and Efg1 (HLC54) were spotted onto the indicated SXD media  
1266 (X = Pro, Arg, Orn or Asp) and incubated at 37 °C for 48 h. **C.** Levels of active GTP bound form  
1267 of Ras1 (Ras1-GTP) increase upon amino acid induction. Extracts were prepared from pooled  
1268 WT (PMRCA18) macrocolonies grown for 24 h at 37 °C on the specified SXD medium. The  
1269 levels of total Ras1 and the activated forms (Ras1-GTP) were determined by  
1270 immunoprecipitation. **D.** Arginine catabolism is required for arginine-induced morphogenesis.  
1271 Cells were spotted on SRD (Arg) supplemented with nor-NOHA, a competitive inhibitor of  
1272 arginase. **E.** Proline catabolism is required for proline-induced morphogenesis. Cells were  
1273 spotted on SPD (Pro) supplemented with L-THFA, a competitive inhibitor of proline  
1274 dehydrogenase. For **D** and **E**, macrocolonies (PMRCA18) were grown at 37 °C and  
1275 photographed after 72 h. Lower images are magnified 2X in comparison to upper images.

1276  
1277 **Fig. 3. Amino acid-induced morphogenesis requires mitochondrial oxidative**

1278 **phosphorylation. A.** ATP levels in macrocolonies (PMRCA18) formed 24 h after spotting cells  
1279 on the indicated SXD medium (X = Asp, Arg, Orn, Pro, Am (ammonium sulfate) or Urea)  
1280 incubated at 37 °C. The levels of ATP in three biological replicates normalized to total protein  
1281 are plotted. The values from each biological replicate is the average of 2-3 technical replicates.  
1282 Statistically significant changes in ATP levels, as compared to cells grown on Asp, are indicated  
1283 (ave. ± CI; \*\*, p value < 0.01; \*, p value < 0.05). **B.** Uncoupling of mitochondria reduces amino  
1284 acid-induced filamentation. Cells (PMRCA18) were spotted on SXD media (X = Arg, Orn or  
1285 Pro) supplemented with indicated amount of methylene blue (MB); macrocolonies were grown  
1286 at 37 °C and photographed after 24 h.

1287  
1288 **Fig. 4. A bifurcated pathway for arginine-induced morphogenesis. A.** Scheme of arginine  
1289 catabolic pathway. **B.** Growth-based assays. Five microliters (5 µl) of serially diluted cells were  
1290 spotted onto the surface of SXD (X = Am (Ammonium sulfate), Arg, Orn, Pro or Urea) and then  
1291 grown for 48 h at 30°C. Strains used: wildtype (WT; PMRCA18), *car1*<sup>-/-</sup> (CFG077), *dur1,2*<sup>-/-</sup>  
1292 (CFG091), *put1*<sup>-/-</sup> (A) (CFG122), *put1*<sup>-/-</sup> (B) (CFG155), and *put1*<sup>-/-</sup> *dur1,2*<sup>-/-</sup> (CFG158). **C.**  
1293 Arginine rapidly derepresses proline catabolic genes. *PUT1*, *PUT2*, *PUT3* and *DUR1,2*  
1294 expression in wildtype (SC5314) cells 1 h at 37 °C after shifting from YPD (t = 0) to YNB+Arg  
1295 (pH = 6.0). Gene expression was determined by qRT-PCR using the levels of *RIP1* to normalize  
1296 expression [96]. **D.** Proline catabolic pathway is required for growth in arginine as a sole nitrogen  
1297 and carbon source. Cells with the indicated genotypes were harvested from log phase YPD  
1298 cultures and diluted in YNB+Arg+BCP medium (pH = 4.0) to OD<sub>600</sub> ≈ 0.01, cultures were  
1299 incubated for 16 h at 37 °C. Alkalinization (shift to purple) correlates with growth. Strains used:  
1300 WT (SC5314), *dur1,2*<sup>-/-</sup> (CFG246), *put1*<sup>-/-</sup> (CFG149), and *put2*<sup>-/-</sup> (CFG143). Identical results  
1301 were obtained using PMRCA18-derived mutants. **E.** Rapid activation of proline catabolism in  
1302 the presence of arginine, ornithine, and proline. Immunoblot analysis of Put2-HA in whole cell  
1303 lysates prepared from CFG185 (*PUT2/PUT2-HA*) cells grown at 37 °C in the specified SXD  
1304 media for the indicated times. Cells were pre-grown in YPD and inoculated at an OD<sub>600</sub> of 0.5.  
1305 Levels of α-tubulin were used to control loading. **F.** Pharmacological inhibition of proline  
1306 dehydrogenase (Put1) reduced filamentous growth of *C. albicans* in the presence of arginine.

1307 Macrocolonies of wildtype (WT; PMRCA18) grown at 37 °C for 72 h on SRD medium  
1308 supplemented with L-THFA as indicated. **G.** Filamentous growth of strains on SXD media (X =  
1309 Arg, Urea, or Arg + Urea as sole nitrogen sources). Macrocolonies were grown at 37 °C and  
1310 photographed at 24 and 48 h. Strains used: wildtype (WT; PMRCA18), *car1*<sup>-/-</sup> (CFG077),  
1311 *dur1,2*<sup>-/-</sup> (CFG091), and *put1*<sup>-/-</sup> (CFG122).

1312  
1313 **Fig 5. Proline utilization is influenced by carbon source but not by NCR.** **A.** Filamentous  
1314 growth is more robust at lower glucose level. Wildtype cells (PMRCA18) from overnight YPD  
1315 liquid cultures were washed and then adjusted to OD<sub>600</sub> of 8, 10 µl aliquots were spotted on  
1316 media containing 10 mM of proline and the indicated levels of carbon source. Plates were  
1317 incubated at 37 °C and photographed at 24, 48 and 72 h. TTC overlay assay was performed on a  
1318 replica plate containing 24 h-old macrocolonies (shown in 24 h panel). **B.** Proline utilization is  
1319 higher under glucose limited conditions. The levels of proline remaining in culture supernatants  
1320 of WT (PMRCA18) after 2 h of growth at 37 °C in the presence of different carbon source, as  
1321 indicated. Results shown are from 5 biological replicates (Ave. ± CI, 95% CL; \*\*\*, p value <  
1322 0.001). Immunoblot analysis of Put2-HA and α-tubulin (loading control) in cell extracts prepared  
1323 from CFG185 (*PUT2/PUT2-HA*) grown under identical conditions (inset). **C.** Respiratory  
1324 growth predominates as glucose level decreases. WT cells were diluted to OD<sub>600</sub> of 0.5 in pre-  
1325 warmed synthetic proline media containing 10 mM proline (YNB+Pro+BCP) and the indicated  
1326 levels of glucose with the initial pH adjusted to 6.0. Cultures were grown for 16 h under vigorous  
1327 agitation at 37 °C prior to photographing the culture tubes. Glycerol was used as respiratory  
1328 growth control. **D.** Put2 is highly expressed in cells grown in the presence of non-glucose carbon  
1329 sources. Immunoblot analysis of cell extracts prepared from CFG185 (*PUT2/PUT2-HA*) cells  
1330 grown in YPGlu (YP+2% glucose = YPD), YPGly (YP + 1% glycerol), YPLac (YP + 1%  
1331 lactate), or Spider medium (with 1% mannitol) at 37 °C for the timepoints indicated. Cells were  
1332 pre-grown in YPD and inoculated at an OD<sub>600</sub> of 0.5. **E.** Proline utilization is insensitive to NCR.  
1333 Immunoblot analysis of cell extracts prepared from CFG184 (*gln3Δ/Δ gat1Δ/Δ PUT2/PUT2-*  
1334 *HA*) grown at 30 °C in SD<sub>0.2%</sub> medium, which contains 10 mM ammonium sulfate (Am) and  
1335 0.2% glucose, supplemented with 10 mM of the nitrogen sources and harvested at the timepoints

1336 as indicated. Cells were pre-grown in SD and then subcultured to log phase in SD<sub>0.2%</sub>.

1337

1338 **Fig 6. Mitochondrial proline catabolism is required by *C. albicans* cells to escape murine**  
1339 **macrophages. A.** Confocal immunofluorescence microscopy of *C. albicans* cells expressing  
1340 Put2-HA (CFG185) in the phagosomes of RAW264.7 macrophages. Primary antibodies (rat anti-  
1341 HA and rabbit anti-Lamp1) and secondary antibodies (Alexa Fluor 555 conjugated goat anti-rat  
1342 antibody and Alexa Fluor 488 conjugated goat anti-rabbit) were used to visualize Put2 and the  
1343 lysosomal compartment, respectively. Orthogonal view of merged channels is shown in the lower  
1344 right panel. Scale bar = 10  $\mu$ . **B.** Proline catabolism is required for hyphal growth of *C. albicans*  
1345 in macrophages. Wildtype (WT; SC5314), heat killed WT, *put1*<sup>-/-</sup> (CFG139), *put2*<sup>-/-</sup> (CFG207),  
1346 *put3*<sup>-/-</sup> (CFG146), *put1*<sup>-/-</sup> *put2*<sup>-/-</sup> (CFG159) and CRISPR/Cas9 control strains CFG181  
1347 (pV1093) and CFG182 (pV1524) pre-grown in YPD and stained with FITC were co-cultured  
1348 with RAW264.7 macrophages at a MOI of 3:1 (C:M). After 30 min, external non-phagocytosed  
1349 cells were removed by washing, and the co-cultures were incubated an additional 4 h. External  
1350 (escaping) hyphal cells were stained with calcofluor white (CFW). Scale bar = 10  $\mu$ . **C.**  
1351 Macrophage killing of *C. albicans*. Strains as in **B** were co-cultured with RAW264.7 at a MOI  
1352 of 3:1 (C:M) for 3 h. After lysing macrophages, viability of *C. albicans* was assessed by  
1353 quantitating the number of CFU. The percent killing was determined by comparison to the  
1354 viability of cells grown in the absence of macrophages.

1355

1356 **Fig 7. Arginine induces morphogenesis in *C. albicans* through mitochondria-dependent**  
1357 **activation of Ras1/cAMP/PKA pathway.** The presence of extracellular arginine enhances  
1358 arginine uptake by binding to the SPS-sensor, leading to the endoproteolytic activation of  
1359 transcription factor Stp2. The active form of Stp2 efficiently targets to the nucleus and binds the  
1360 UAS<sub>aa</sub> in the promoter of genes encoding amino acid permeases (*AAP*). Amino acid permeases  
1361 are cotranslationally inserted into the membrane of the ER, and transported to the plasma  
1362 membrane (PM, arrow) via the secretory pathway, a process that requires the ER membrane-  
1363 localized chaperone Csh3. The increased functional expression of amino acid permeases (Aap)

1364 lead to an enhanced capacity to take up arginine. Intracellular arginine is catabolized by arginase  
1365 (Car1) yielding ornithine and urea. Urea is further degraded by the urea amidolyase (Dur1,2)  
1366 generating CO<sub>2</sub> and NH<sub>3</sub>. Ornithine is further catabolized to proline in the cytoplasm in a series  
1367 of enzymatic reactions starting with the ornithine aminotransferase (Car2). Proline is transported  
1368 into the mitochondria where it is catabolized by Put1 and Put2 forming glutamate. These  
1369 reactions generate the reduced electron carriers FADH<sub>2</sub> and NADH,H<sup>+</sup>, respectively. Glutamate  
1370 is oxidized by glutamate dehydrogenase (Gdh2) forming  $\alpha$ -ketoglutarate in a reaction that  
1371 liberates NH<sub>3</sub> and generates NADH,H<sup>+</sup>.  $\alpha$ -ketoglutarate feeds directly into the mitochondria-  
1372 localized TCA cycle. The reduced electron carriers generated by proline, glutamate and TCA  
1373 cycle metabolic events are oxidized in reactions coupled to the generation ATP by mitochondrial  
1374 oxidative phosphorylation. The elevated levels of ATP in the cytoplasm activate the adenyl  
1375 cyclase (Cyr1) in a Ras1-dependent manner, which activates the downstream protein kinase A  
1376 (PKA) signaling pathway and the effector transcription factor Efg1. The active phosphorylated  
1377 form of Efg1 binds the UAS<sub>Efg1</sub> in the promoter of hyphal specific genes (*HSG*), thereby inducing  
1378 yeast-to-hyphal morphogenesis. The catabolism of arginine via the proline pathway induces  
1379 hyphal growth more rapidly (FAST) than the Dur1,2 generated CO<sub>2</sub> (slow). Mitochondrial  
1380 activity is repressed in the presence of high glucose.

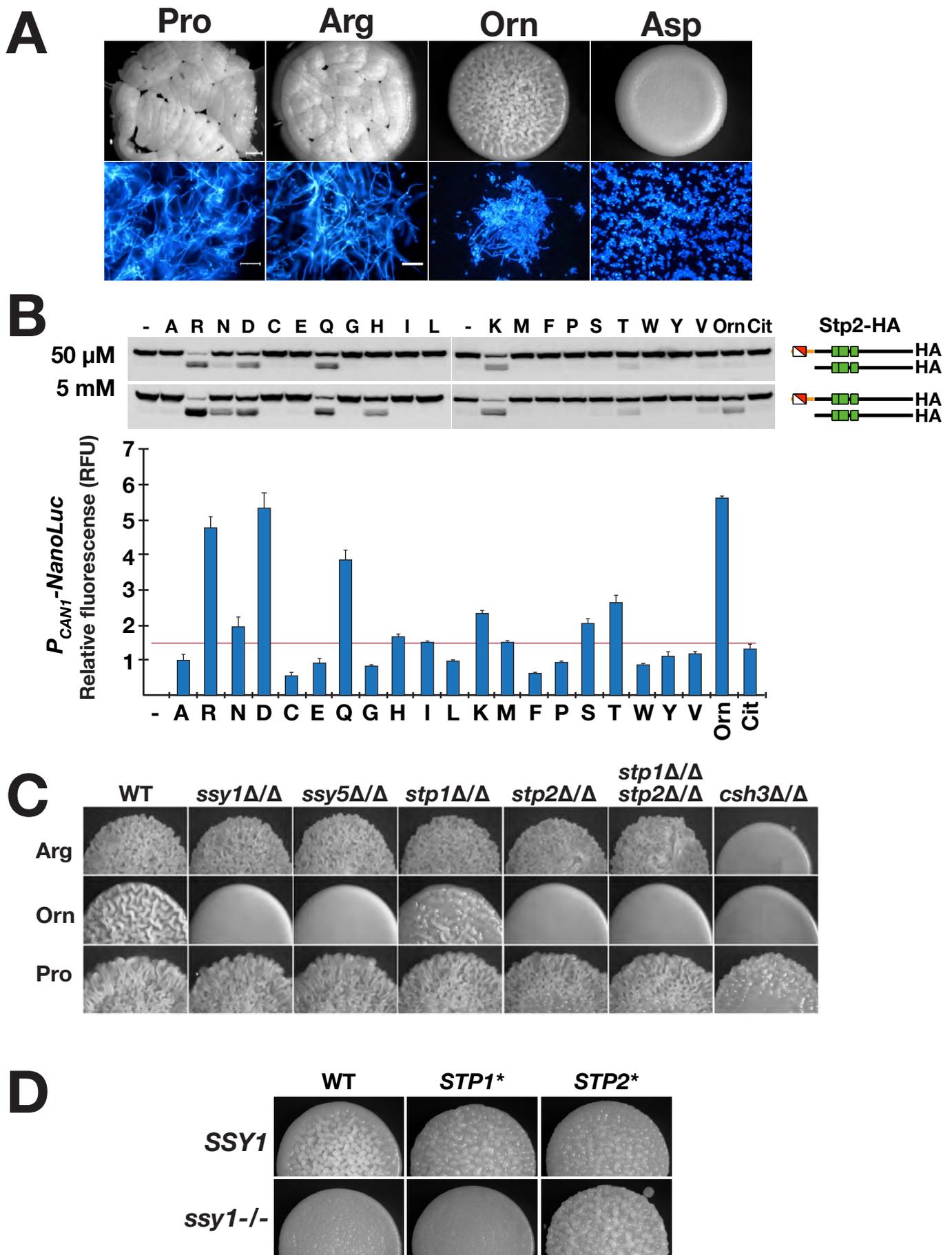


Fig. 1 Silao et al.

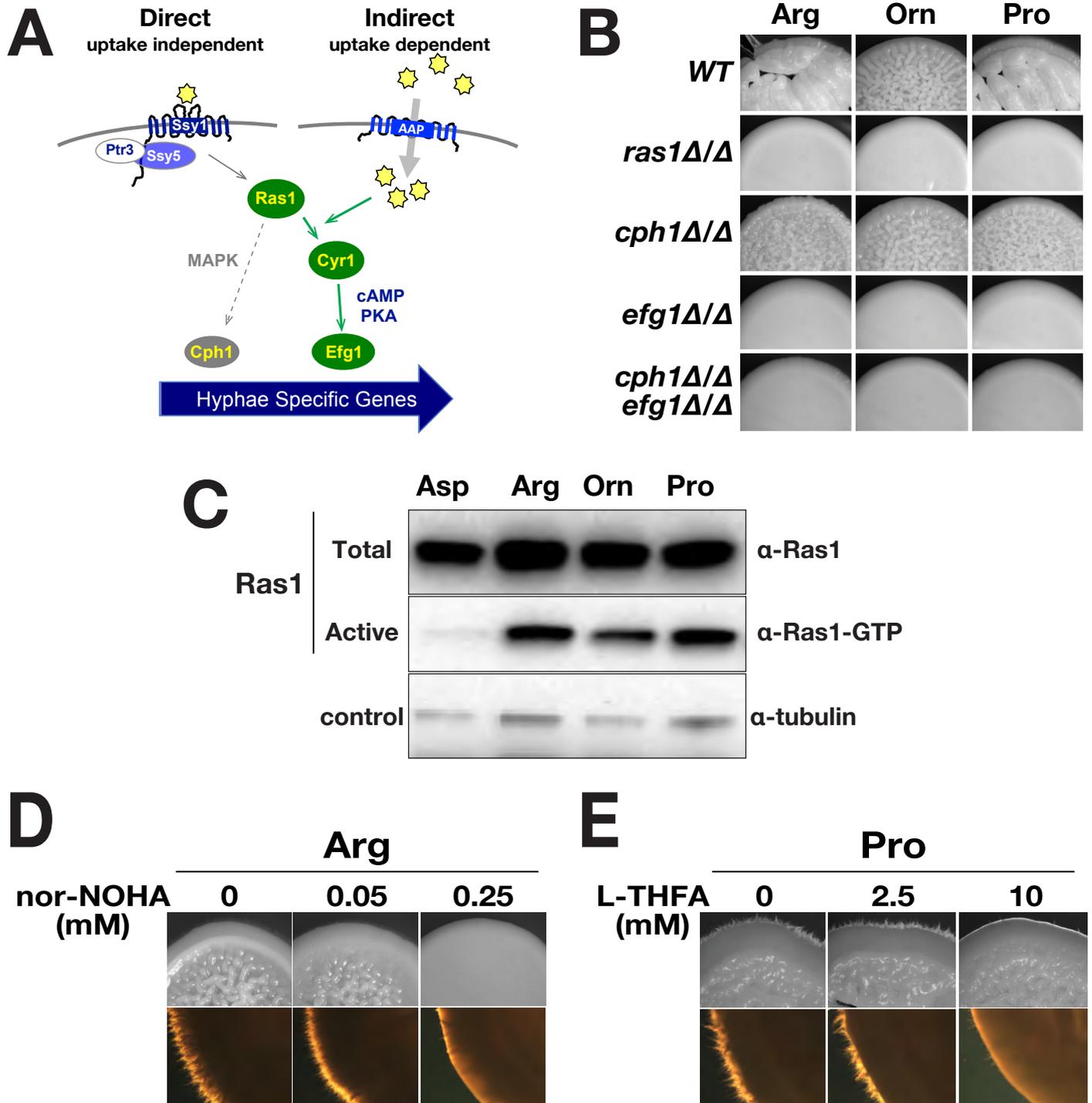


Fig. 2 Silao et al.

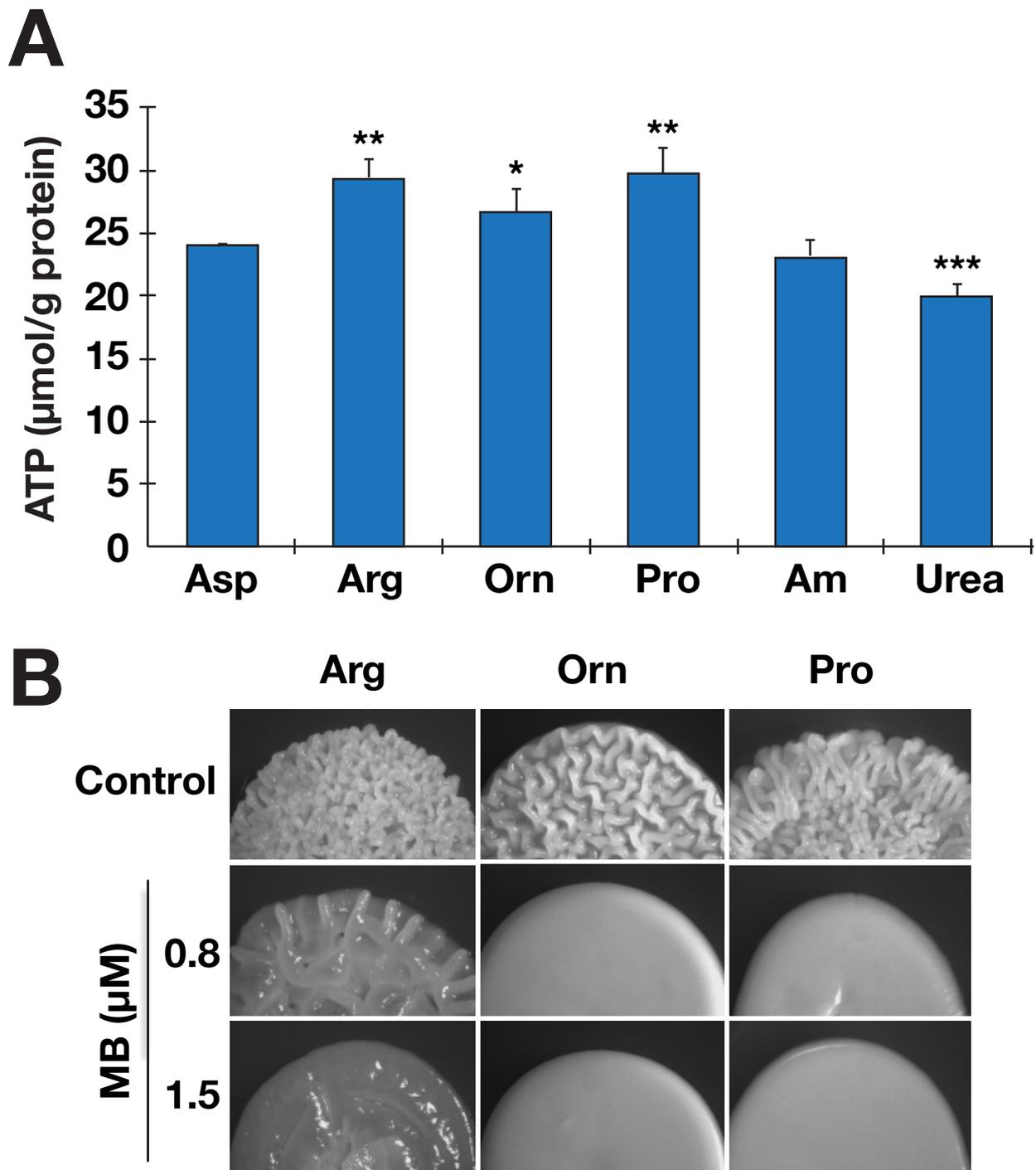


Fig. 3 Silao et al.

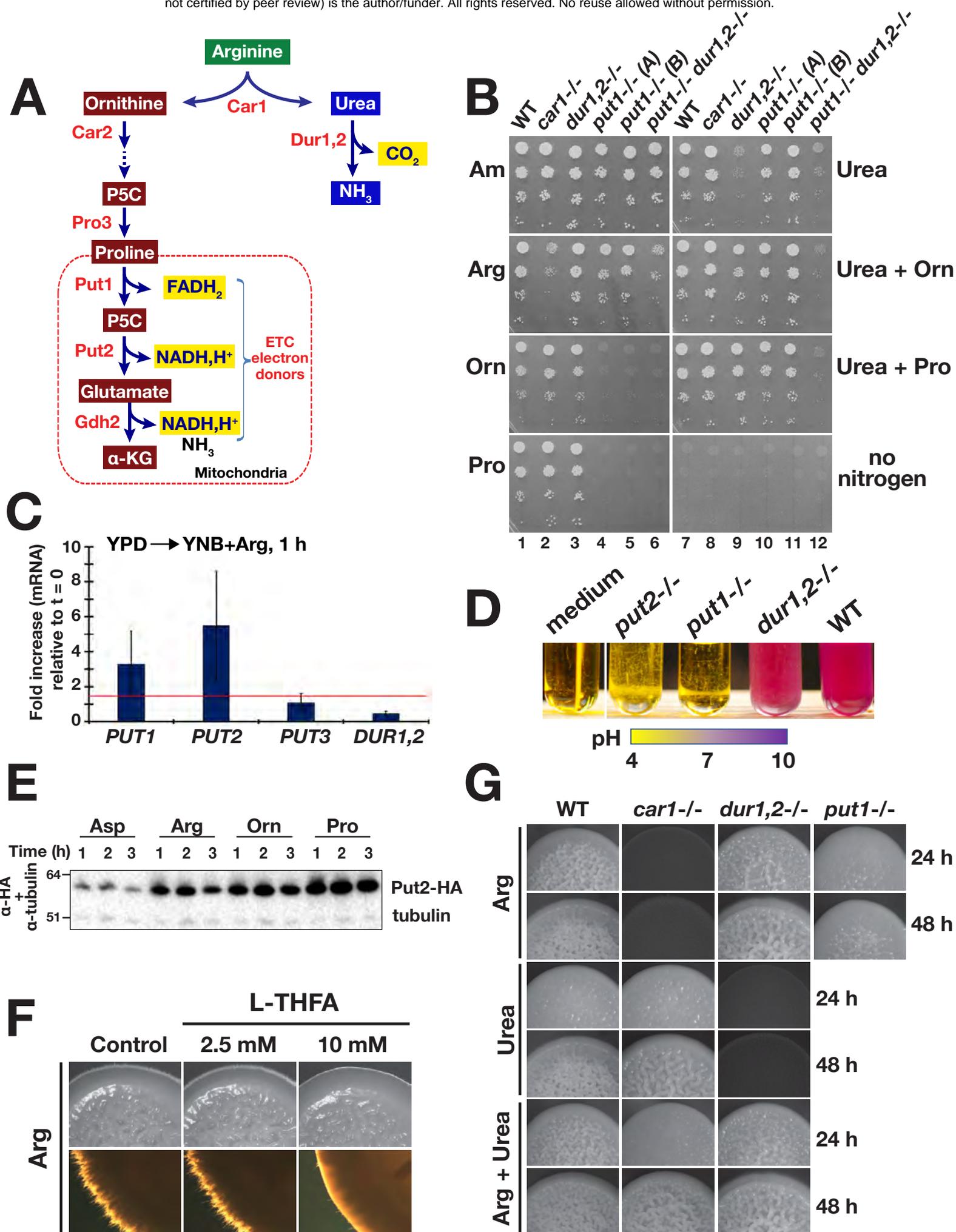


Fig. 4 Silao et al.

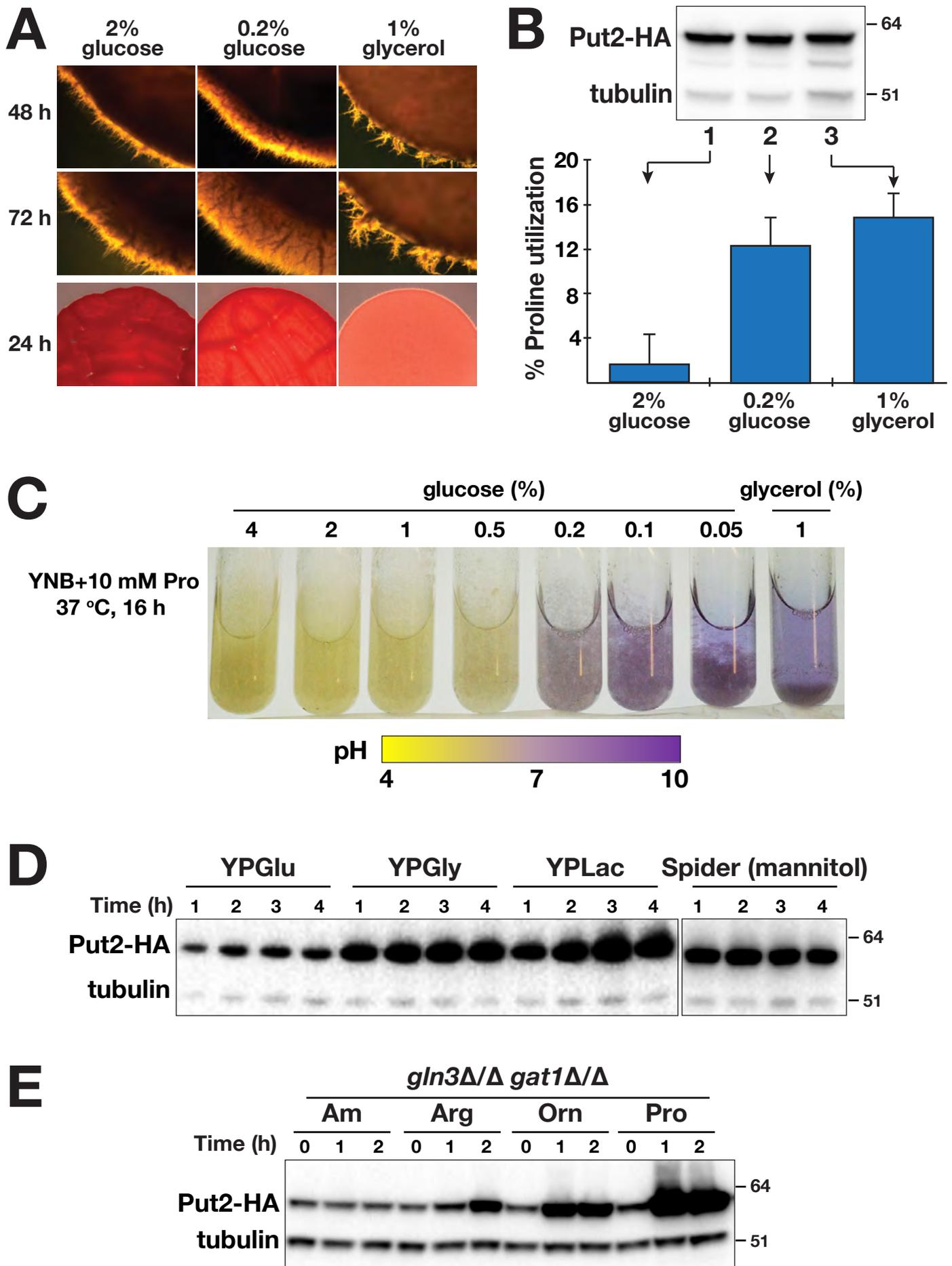


Fig. 5 Silao et al.

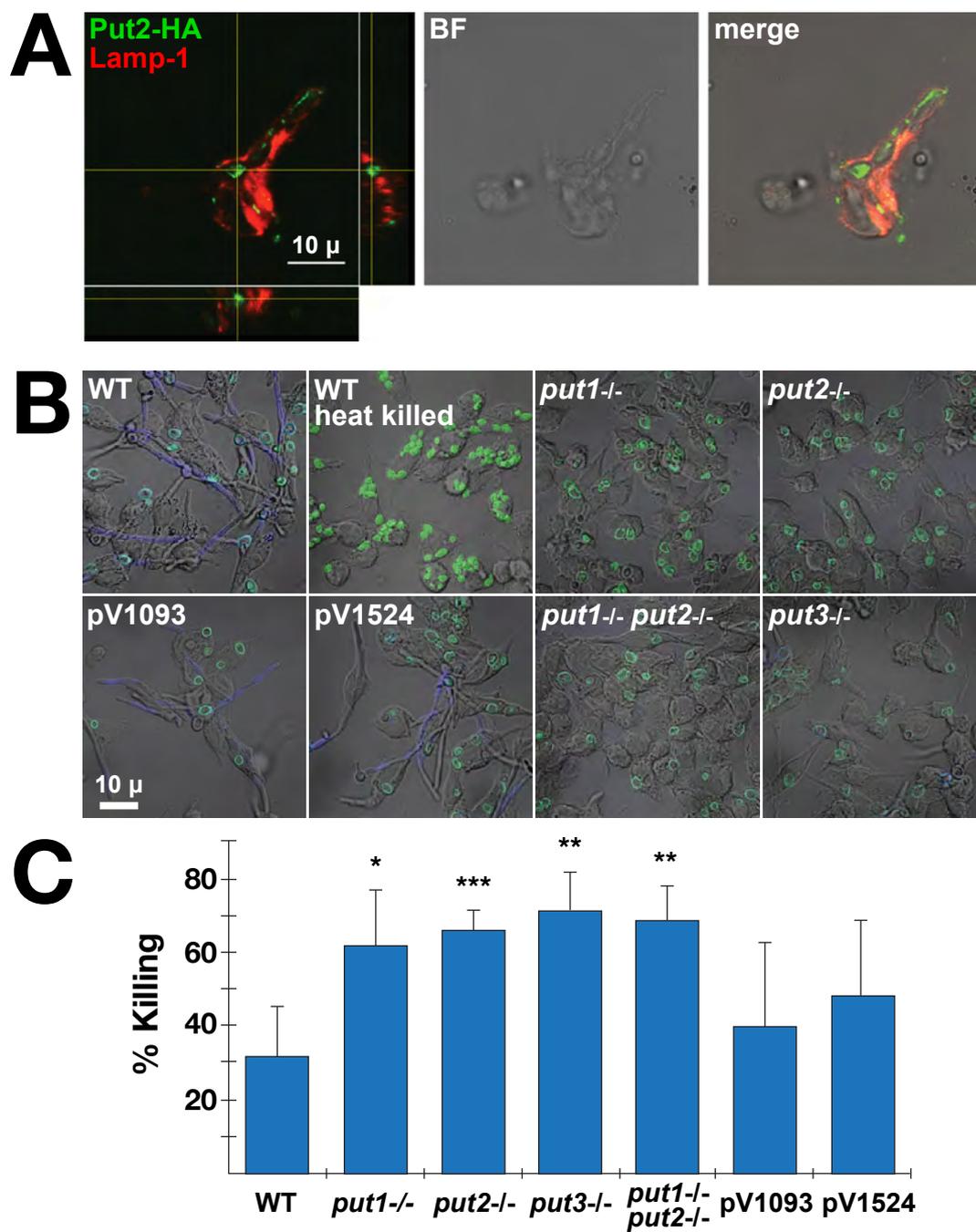


Fig. 6 Silao et al.

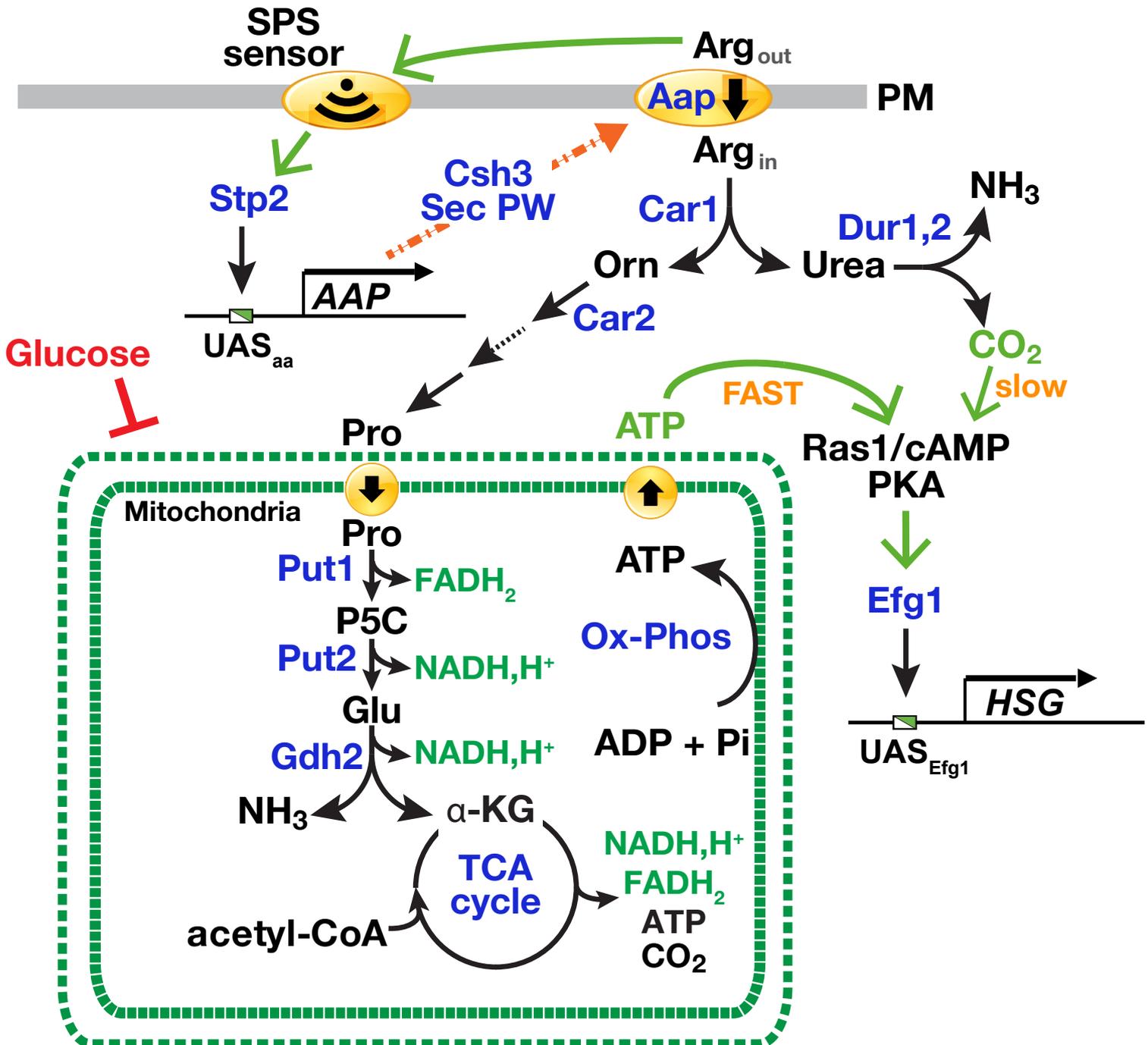


Fig. 7 Silao et al.